Journal of Medicinal Chemistry

Article

Cite This: J. Med. Chem. XXXX, XXX, XXX−XXX

pubs.acs.org/jmc

Application of Sequential Palladium Catalysis for the Discovery of Janus Kinase Inhibitors in the Benzo[*c*]pyrrolo[2,3-*h*][1,6]naphthyridin-5-one (BPN) Series

Mohamed S. A. Elsayed,[†,§] Jeffery J. Nielsen,[†,§] Sungtae Park,[‡,§] Jeongho Park,[‡,§] Qingyang Liu,[‡,∥] Chang H. Kim,[‡,§,∥] Yves Pommier,[⊥] Keli Agama,[⊥] Philip S. Low,[#,§] and Mark Cushman*[,†,§]

[†]Department of Medicinal Chemistry and Molecular Pharmacology, College of Pharmacy, Purdue University, West Lafayette, Indiana 47907, United States

[‡]Department of Comparative Pathobiology, College of Veterinary Medicine, Purdue University, West Lafayette, Indiana 47907, United States

[§]The Purdue Center for Cancer Research, Purdue University, West Lafayette, Indiana 47907, United States

[∥]Department of Pathology and Mary H. Weiser Food Allergy Center, University of Michigan Medical School, Ann Arbor, Michigan 48109, United States

[⊥]Developmental Therapeutics Branch and Laboratory of Molecular Pharmacology, Center for Cancer Research, National Cancer Institute, Bethesda, Maryland 20892, United States

[#]Department of Chemistry, Purdue University, West Lafayette, Indiana 47907, United States

Supporting Information

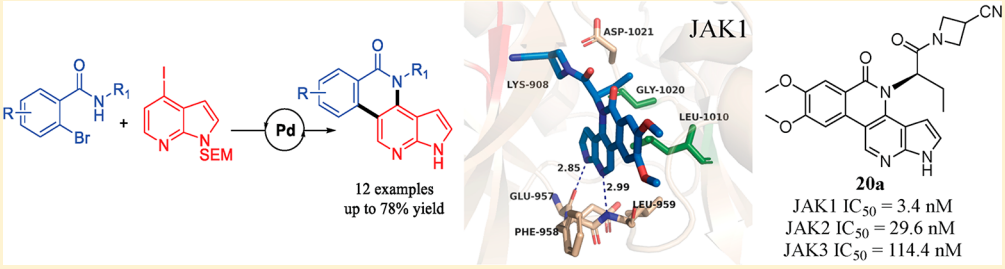

ABSTRACT: The present account describes the discovery and development of a new benzo[*c*]pyrrolo[2,3-*h*][1,6]-naphthyridin-5-one (BPN) JAK inhibitory chemotype that has produced selective JAK inhibitors. Sequential palladium chemistry was optimized for the rapid access to a focused library of derivatives to explore the structure−activity relationships of the new scaffold. Several compounds from the series displayed potencies in the low nanomolar range against the four members of the JAK family with various selectivity profiles. Compound **20a**, with an azetidine amide side chain, showed the best selectivity for JAK1 kinase vs JAK2, JAK3, and TYK2, with low nanomolar potency (IC_{50} = 3.4 nM). On the other hand, BPNs **17b** and **18** had good general activity against the JAK family with excellent kinome selectivity profiles. Many of the new BPNs inhibited JAK3-mediated STAT-5 phosphorylation, the production of inflammatory cytokines, and the proliferation of primary T cells. Moreover, BPN **17b** showed very similar in vivo results to tofacitinib in a rheumatoid arthritis animal model.

INTRODUCTION

The human immune response is a very complex process involved in defense against external pathogens and foreign tissues.[1] Abnormalities of the immune system often lead to disease states such as cancer and autoimmune disorders.[2] In autoimmune diseases, the immune system attacks tissues within the same organism. It is estimated that 24 million people are affected by autoimmune diseases in the United States.[3] Cytokines regulate the immune responses by mediating gene activation and repression.[4] The JAK-STAT pathway plays a central role in the signal transduction cascades of many cytokines (Figure 1).[5]

As shown in Figure 1A, cytokine binding triggers receptor dimerization, which leads to JAK tyrosine kinase activation in which the two JAKs phosphorylate each other on a tyrosine residue in the activation loop. JAK-mediated STAT phosphorylation subsequently induces dimerization of the STAT signal transduction proteins and their translocation to the nucleus, which initiates gene transcription.[5] The JAK family has four members: JAK1, JAK2, JAK3, and TYK2.[6] The JAKs are activated in various patterns by different cytokines (Figure 1B). JAK1 and JAK3 are activated by the members of the γ

Received: March 31, 2018

DOI: 10.1021/acs.jmedchem.8b00510
J. Med. Chem. XXXX, XXX, XXX−XXX

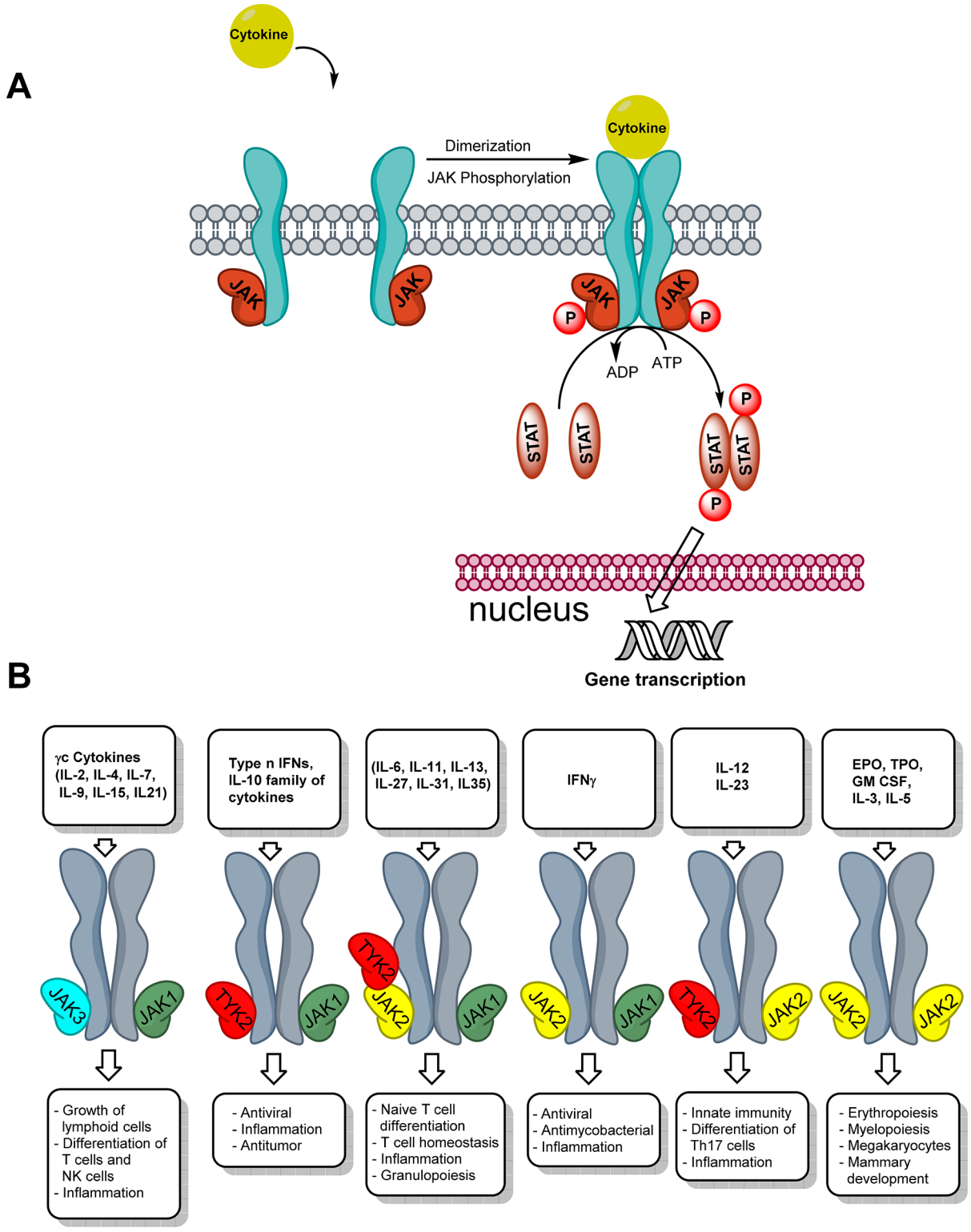

Figure 1. (A) The JAK-STAT signaling pathway; (B) various biological responses mediated through the JAK pathway.[7]

common (γ_c) subfamily, namely interleukins IL-2, IL-4, IL-7, IL-9, IL-15, and IL-21, which cannot activate JAK2 or TYK2. On the other hand, another subfamily of cytokines that includes IL-6, IL-11, and IL-17 binds to unique receptors that share a common glycoprotein 130 (gp130) subunit that is required for downstream JAK signaling. Several other cytokines induce JAK1 activation, and JAK2 and TYK2 are also consistently activated. Erythropoietin (EPO) receptors are another subfamily of homodimeric receptors that also includes the receptors for prolactin, thrombopoietin, and growth hormone. The EPO pathway activates JAK2 exclusively and is essential for erythropoiesis.

Extensive efforts have been expended over the past decade to identify novel small-molecule JAK inhibitors with various subtype selectivity profiles to address unmet medical needs presented by transplant rejection, rheumatoid arthritis, other

DOI: 10.1021/acs.jmedchem.8b00510
J. Med. Chem. XXXX, XXX, XXX−XXX

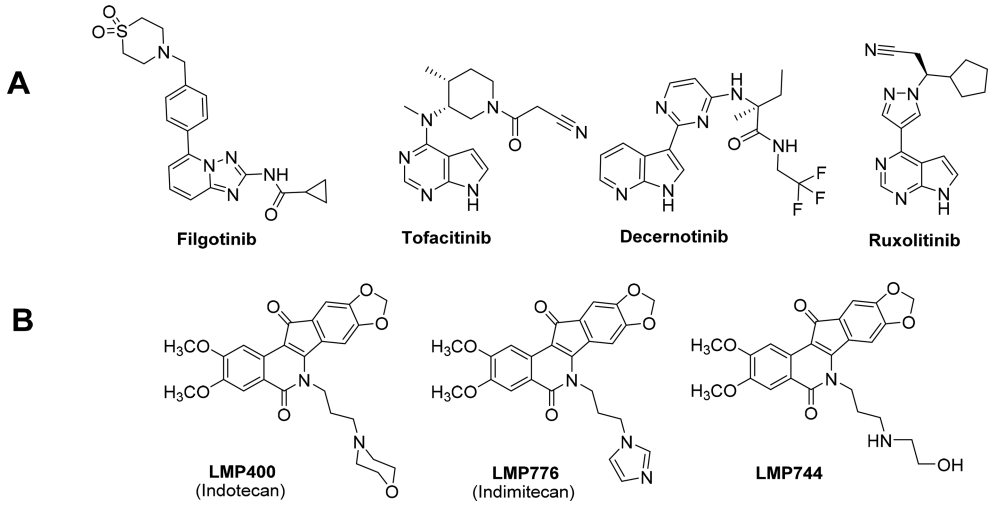

Figure 2. Examples of JAK inhibitors (A) and topoisomerase I poisons (B).

autoimmune diseases, and cancer.[7] The structures of four JAK inhibitors currently approved or in clinical trials are displayed in Figure 2A.

The currently approved drugs are mixed inhibitors of all four JAK kinases with varying potencies against each one.[8] Tofacitinib is approved by the FDA for the treatment of rheumatoid arthritis, psoriatic arthritis, and ulcerative colitis, while ruxolitinib is approved for the treatment of myelofibrosis and polycythemia vera.[9] These two JAK inhibitors suffer from many side effects, arguing that more selective medications should be developed to overcome them.[9,10]

Palladium catalysis has offered new pathways for the preparation of pharmaceuticals.[11] Tandem catalysis is a process in which the catalyst is used to catalyze more than one reaction for the construction of complex molecules from simple building blocks.[12] In the present work, autotandem palladium catalysis was applied for the rapid construction of pharmacologically active JAK inhibitors. This approach has made the synthesis of these compounds easier, and it has allowed rapid diversification of newly designed scaffolds to obtain a wide range of derivatives with various activities and selectivities.[13]

Design and Discovery. Potentiation of the effect of topoisomerase I (Top1) inhibition by checkpoint kinase (Chk1) inhibitors has been previously demonstrated for the combination of various Chk1 inhibitors and camptothecin, and it has also been shown for Chk1 siRNA.[14] A selective Chk1 inhibitor also displayed dose-dependent potentiation of the antitumor effect of irinotecan in MDA-MB-435 breast cancer xenografts.[15] Several other studies showed the potentiating effect of Chk1 inhibitors on DNA-acting anticancer agents, including Top1 inhibitors.[16,17] For example, Aris et al. reported the potentiation of the cellular effect of LMP400 by the cell checkpoint and Chk1-Chk2 inhibitor AZD7762.[18] This encouraged us to attempt the design of potential dual Top1/Chk1 kinase inhibitors.

Analogues of our Top1 inhibitors LMP400, LMP776, and LMP744 (Figure 2B) that have been in phase I clinical trials were designed in an effort to make compounds with dual Top1 and Chk kinase inhibitory activity (Figure 3). The design was guided by the structural similarities between the reported pyrazoloquinoline class of potent Chk1 inhibitors[19] represented in Figure 3 and the indenoisoquinolines. Both structures have a flat scaffold, a hydrogen bond acceptor that

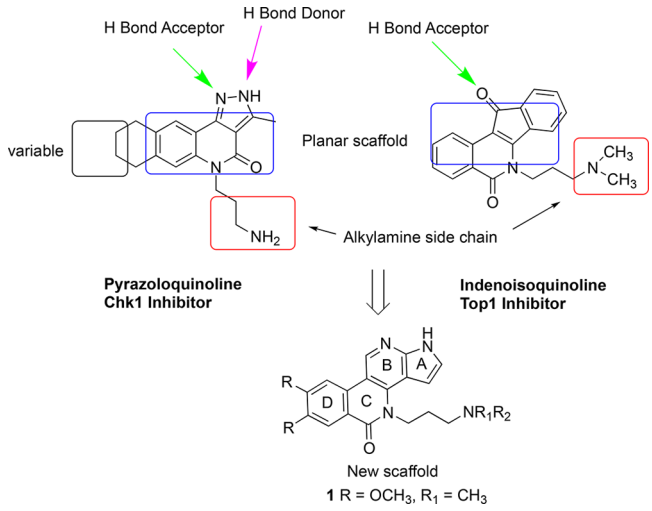

Figure 3. Design rationale for the BPN **1** scaffold. The structural similarity between the two compounds was used in the design. The indenoisoquinoline scaffold was modified by adding an additional hinge-binding element (hydrogen bond donor) to the hydrogen bond acceptor, which was changed from a carbonyl oxygen to the pyridine nitrogen. At the same time, the basic aminopropyl side chain was retained.

can be oriented in the same direction, and a basic aminopropyl side chain. Hybridization of the two structures and addition of the missing hydrogen bond donor required for hinge binding of kinase inhibitors resulted in the structure of compound **1** as shown in Figure 3.

BPN **1** was prepared (Scheme 1) and tested against both Chk1 kinase and Top1 and also for cytotoxic activity. It had mild Chk inhibitory activity and no Top1 inhibitory activity. However, BPN **7b** had selectivity against blood cancer cell lines in the cytotoxicity assay (Supporting Information). BPN **1** was therefore tested against a focused library of related tyrosine kinases that were selected on the basis of a similarity search using the ChEMBL database.[20]

Kinase profiling of BPN **1** against nine kinases suggested by the similarity search revealed that it has very good affinity and some selectivity against JAK kinases (Table 1). Binding assays of **1** showed high affinities with a K_d = 20 nM against JAK3 and a K_d = 19 nM against JAK2 kinases. This scaffold is a new JAK

DOI: 10.1021/acs.jmedchem.8b00510
J. Med. Chem. XXXX, XXX, XXX−XXX

Table 1. Enzyme Affinity Data for BPN 1 against Nine Kinases

kinase	%Ctrl @ 10 μM[a]
CDK2	100
Chk1	15
Chk2	5.2
EGFR	83
JAK1	5.8
JAK2	0
JAK3	0
MET	19
VEGFR-2	7.5

[a]Values were obtained by comparing the results of the test compounds to a negative control that was assigned a value of 100% (nonbinding). Lower numbers indicate stronger binding.

inhibitory chemotype that encouraged the further exploration of it to see if new JAK inhibitors could be obtained with optimized activity. The design may be considered as an extension of the polycyclic JAK inhibitors that have been reported in the literature.[21−24] These BPNs were conceived as conformationally constrained relatives of tofacitinib that would direct the placement of the side chain in the binding pocket.

The molecular model in Figure 4 shows the predicted binding mode of BPN **1** in the ATP binding site of JAK3 overlapped with tofacitinib. On the basis of the molecular modeling and comparison with other JAK inhibitors, a series of modifications were made to BPN **1** to explore the SAR. The azaindole fragment in the new scaffold keeps the essential hinge binding element by forming two hydrogen bonds with Glu903 and Leu905. The side chain in BPN **1** is basic in nature, which often causes problems of nonselective kinome and hERG binding. Initially, the basic side chain was replaced with simple side chains like the esters as in BPNs **13a−c** (Scheme 2). These side chains were originally designed to test whether the binding site can enclose esters and larger groups of this chemical nature. Afterward, BPNs such as **17a−d** with hydrophobic and alicyclic groups similar to the reported inhibitors were also considered (BPNs **17a−d**, Scheme 3). Cyclic amines have been reported to be present in some selective JAK inhibitors, and therefore similar side chains were incorporated in the new scaffold (BPNs **17e−h**).[25,26] A tofacitinib-like side chain was also incorporated to compare the resulting product to the clinically used compound (BPN **18**, Scheme 5). Finally, the chirality of amino acids was harnessed to make the chiral BPNs **19−21** with amide side chains to target the two different sides of the binding pocket.[27]

Chemistry. Initially, the synthetic pathway illustrated in Scheme 1 was investigated for the synthesis of BPN **1** and two more analogues **7a** and **7b** with unsubstituted or with a nitro-substituted ring D. Compound **2** was protected with MOMCl using NaH in DMF according to literature methodology.[28] Buchwald chemistry was used to add the amine side chain to afford compound **4**. The appropriate 2-bromobenzoic acid derivatives are commercially available and were used for the synthesis of compounds **5a−c**. Each acid was heated at reflux in $SOCl_2$ to obtain the acid chlorides, which were reacted with compound **4** in DCM and TEA. The direct intramolecular arylation reaction was used to obtain compounds **6a−c**. The yield of this reaction was improved by replacing cesium carbonate with potassium carbonate. Finally, compounds **1** and **7a**,**b** were obtained by removing the MOM group by heating in concentrated HCl in THF.

The synthetic methodology used in Scheme 1 was not very useful for the synthesis of the second batch of compounds with altered side chains because increasing the size of the amine substituents hindered amide formation with the acid chloride. Scheme 2 illustrates an alternate synthetic pathway used for the synthesis of BPNs **13a−c**. First, the protected azaindole compound **8**[29] was converted to the amine **9** using Buchwald chemistry with benzophenone imine and palladium acetate. The amine **9** was reacted with the required 2-iodoacyl chloride derivative to provide the common intermediate **10**, which was alkylated with various reactants using sodium hydride in DMF to afford **11a−c**. An intramolecular ring coupling reaction yielded intermediates **12a−c**, which were easily deprotected by TFA to give the target compounds **13a−c**.

The two schemes used for the synthesis of the target BPNs were highly convergent, but they were not successful in making compounds with bulkier side chains as, for example, a cyclohexyl group. Also, the application of the second scheme was limited to reactants that have an α-carbonyl relative to the halide atom that facilitates the S_N2 reaction. To widen the

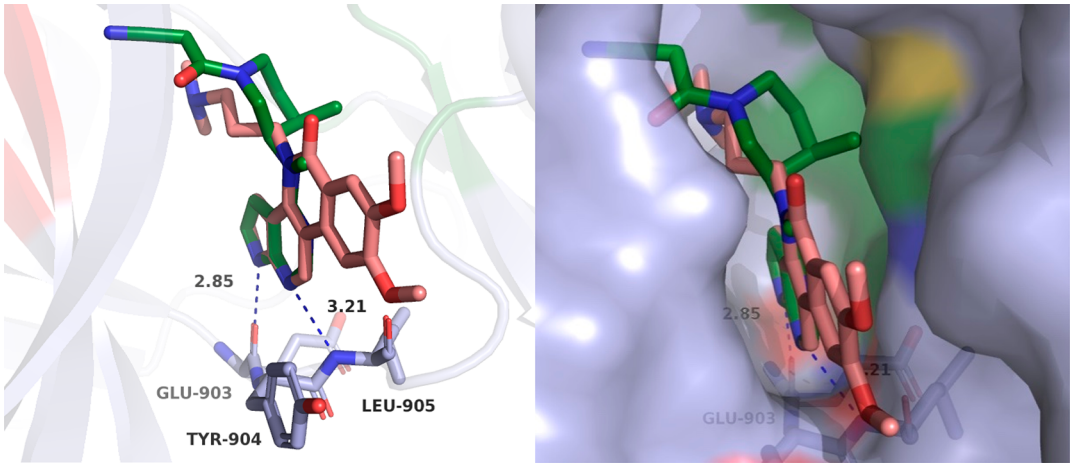

Figure 4. Binding mode of compound **1** (orange) aligned with tofacitinib (green) in the active site of JAK3 (PDB 3LXK). A surface representation to the right illustrates the binding mode of the side chain of compound **1** and tofacitinib. The green area represents the methyl pocket occupied by the tofacitinib side chain.

DOI: 10.1021/acs.jmedchem.8b00510
J. Med. Chem. XXXX, XXX, XXX−XXX

Scheme 1[a]

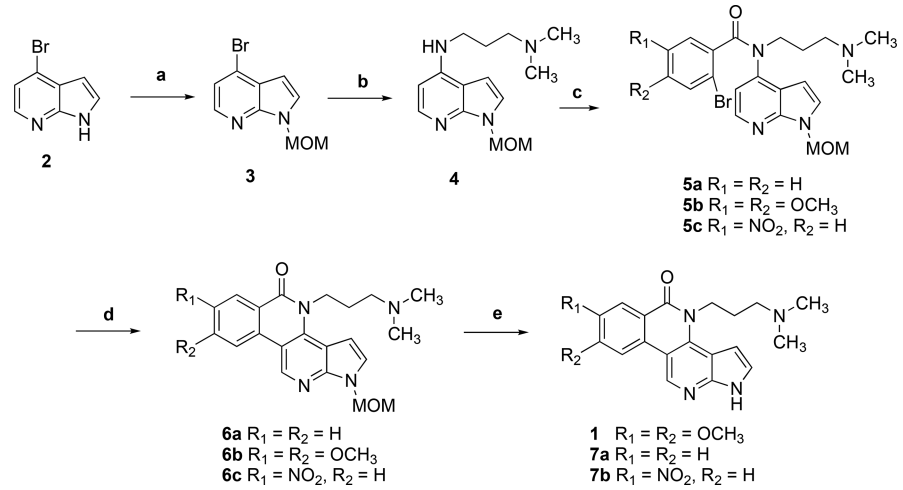

[a](a) MOMCl, NaH, DMF, 0– 21 °C, 3 h; (b) $(H_3C)_2NCH_2CH_2CH_2NH_2$, $Pd_2(dba)_3$, xantphos, Cs_2CO_3, dioxane, 110 °C, 16 h; (c) ArCOCl, TEA, CH_2Cl_2, 0–60 °C, 5 h; (d) $Pd(OAc)_2$, K_2CO_3, $PCy_3{\cdot}HBF_4$, DMA, 130 °C, 18 h; (e) concd HCl, THF, 60 °C, 20 h.

Scheme 2[a]

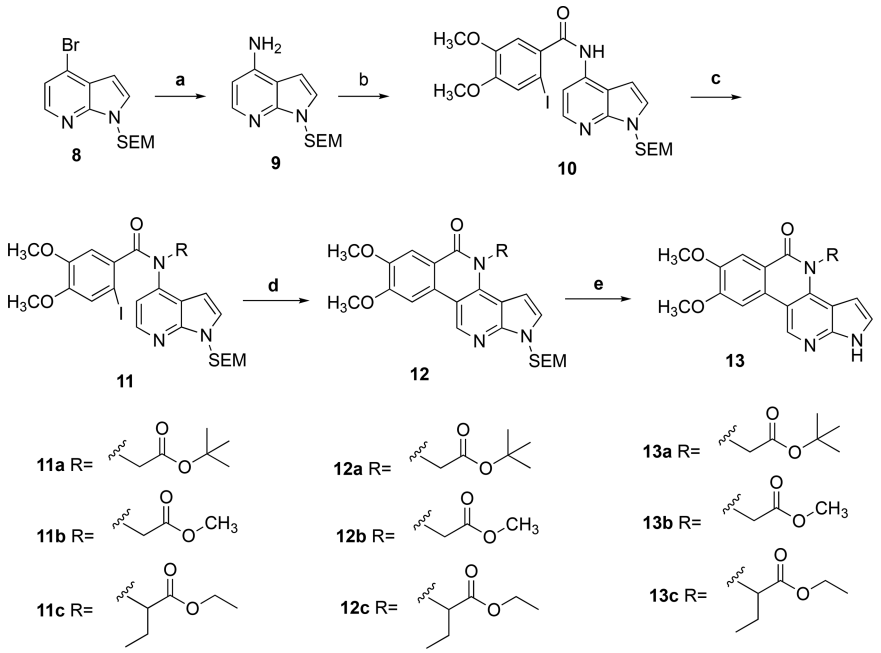

[a](a) (i) $Pd(OAc)_2$, benzophenone imine, Cs_2CO_3, xantphos, dioxane, 110 °C, (ii) $NH_2OH{\cdot}HCl$, NaOAc, MeOH, 21 °C; (b) ArCOCl, TEA, CH_2Cl_2, 23 °C, 16 h; (c) R-Br, NaH, DMF, 21 °C, 18 h; (d) $Pd(OAc)_2$, $PCy_3{\cdot}HBF_4$, K_2CO_3, DMA, 130 °C, 18 h; (e) (i) TFA, CH_2Cl_2, (ii) ethylenediamine, NaOH, MeOH.

range of side chains and facilitate scaffold decoration, a new tandem Pd reaction was engineered that can achieve the Buchwald amidation and the intramolecular arylation in just one step.

The reaction portrayed in Table 2 is a modification of the Catellani reaction in which the bifunctionalization of aryl halides is facilitated by norbornene. The original conditions reported by Catellani and co-workers failed to provide the required compound in a good yield.[30] The aryl iodide in the present case is different from *o*-iodotoluene in the original paper. In addition to optimizing the yield, the versatility of the reaction needed to be augmented in order to facilitate the synthesis of a broad range of JAK inhibitors. The conditions of the Catellani reaction were therefore optimized as reported in Table 2.

The use of DMA as the solvent and PPh_3 as the ligand (entry 4) was not optimal for the reaction as the yield was only 4%. After further investigation of the solvent effect, toluene was found to be the best one with 56% yield (entry 9). The use of potassium carbonate as the base proved to be ineffective, as shown in entries 1–4. After some trials, cesium carbonate was established to be the best base for the reaction with 68% yield (entry 9). TFP [tri(2-furyl)phosphine] provided optimal yields relative to the other ligands that were investigated. Finally, palladium acetate was replaced with palladium trifluoroacetate and this enhanced the yield. Palladium trifluoroacetate has

DOI: 10.1021/acs.jmedchem.8b00510
J. Med. Chem. XXXX, XXX, XXX–XXX

Table 2. Optimization of the Catellani Reaction

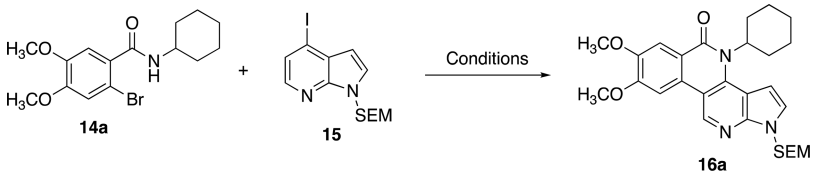

entry*	catalyst	ligand	base	solvent	additive	temp (C°)/time (h)	yield (%)[a]
1	$Pd(OAc)_2$	TFP[b]	K_2CO_3	CH_3CN		85/18	<2
2	$Pd(OAc)_2$	TFP	K_2CO_3	DMF		105/18	0
3	$Pd(OAc)_2$	TFP	K_2CO_3	CH_3CN	norbornene	100/18	20
4	$Pd(OAc)_2$	PPh_3	K_2CO_3	DMA	norbornene	130/18	4
5	$Pd(OAc)_2$	TFP	Cs_2CO_3	CH_3CN	norbornene	85/18	24
6	$Pd(OAc)_2$	TFP	Cs_2CO_3	dioxane	norbornene	95/18	21
7	$Pd(OAc)_2$	TFP	Cs_2CO_3	THF	norbornene	70/18	34
8	$Pd(OAc)_2$	TFP	*t*-BuOK	toluene	norbornene	100/18	56
9	$Pd(OAc)_2$	TFP	Cs_2CO_3	toluene	norbornene	100/18	68
10	$Pd(OAc)_2$	TFP	*t*-BuOK	tol/CH_3CN	norbornene	100/18	68
11	$Pd(OAc)_2$	xantphos	Cs_2CO_3	tol/CH_3CN	norbornene	100/18	52
12	$Pd(OAc)_2$	$PCy_3{\cdot}HB_4$	Cs_2CO_3	tol/CH_3CN	norbornene	100/18	42
13	$Pd(OAc)_2$	S-Phos	Cs_2CO_3	tol/CH_3CN	norbornene	100/18	32
14	$Pd_2(dba)_3$	TFP	Cs_2CO_3	toluene	norbornene	100/18	70
15	$Pd(TFA)_2$	TFP	Na_2CO_3	toluene	norbornene	100/8	75
16	**$Pd(TFA)_2$**	**TFP**	**Cs_2CO_3**	**toluene**	**norbornene**	**100/20**	**78**

[a]All the numbers are the isolated yields. [b]Tri(2-furyl)phosphine.

Scheme 3[a]

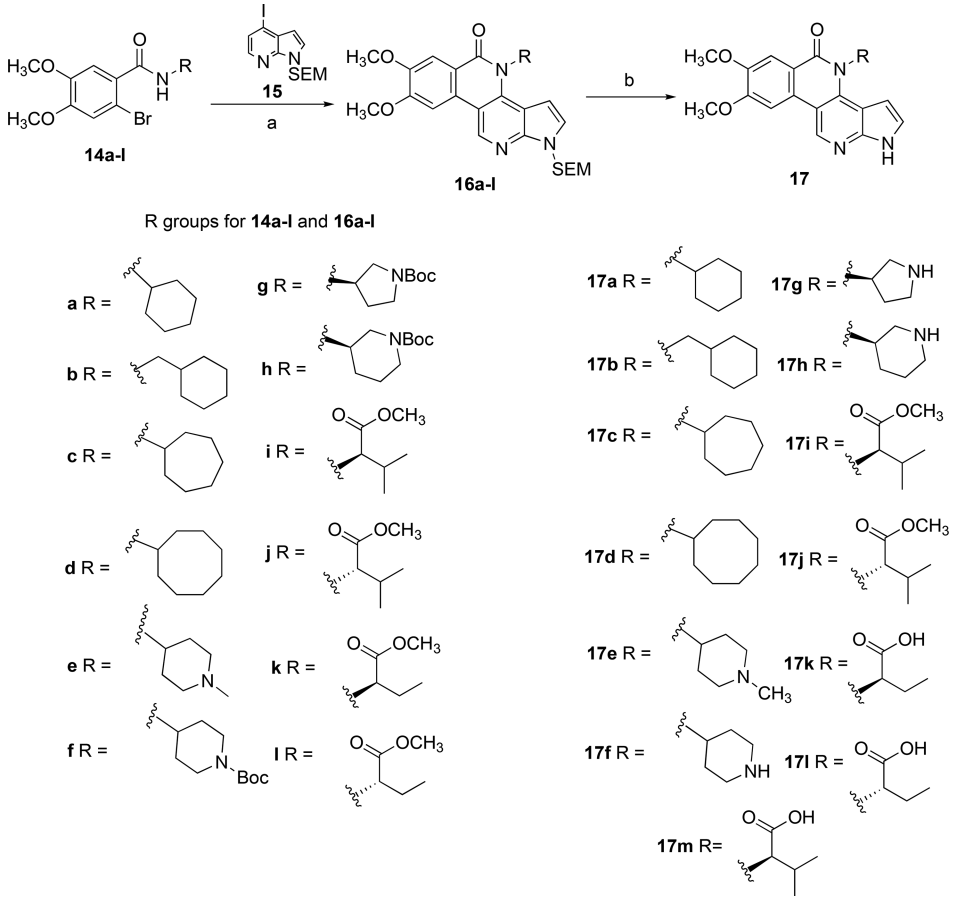

[a](a) $Pd(TFA)_2$, Cs_2CO_3, norbornene, TFP, toluene, 110 °C; (b) (i) TFA, (ii) $H_2N(CH_2)_2NH_2$ or (i) TFA, (ii) NaOH.

DOI: 10.1021/acs.jmedchem.8b00510
J. Med. Chem. XXXX, XXX, XXX−XXX

Scheme 4

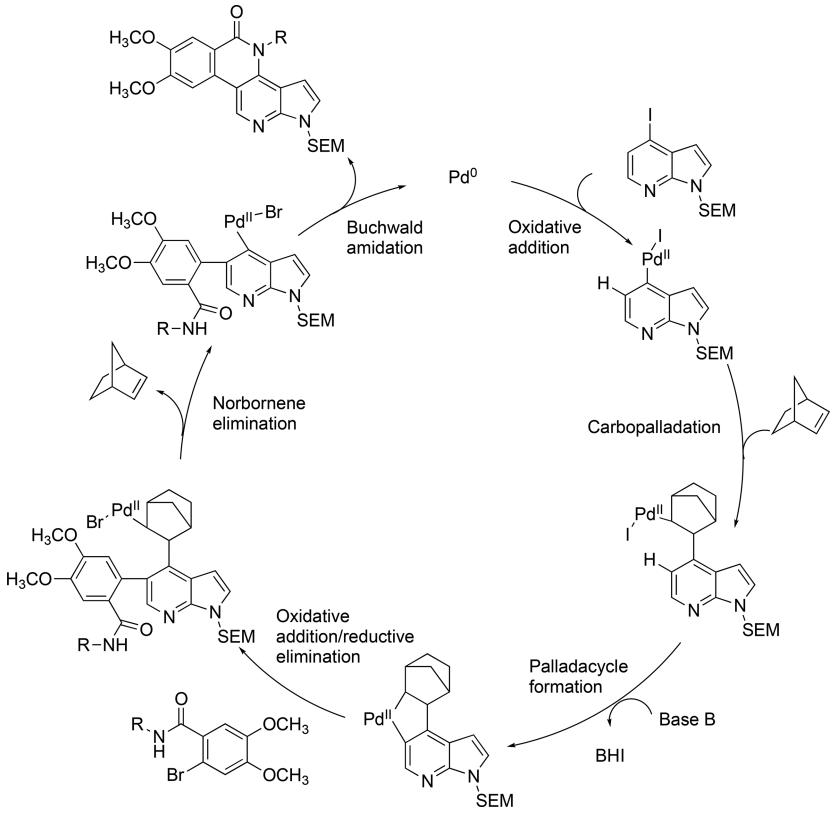

been reported to be more efficient than palladium acetate in nonpolar solvents like toluene.[31,32]

Scheme 3 illustrates the new reaction and the versatility of side chain installation that it provides. In this reaction, the amides **14a−l** were reacted with the iodo compound **15** to form both of the new C−N and C−C bonds and generate compounds **16a−l** in a single step instead of the four steps employed in Scheme 1. The amides **14a−l** can be easily obtained from the commercially available *o*-bromo acids, and compound **15** can be prepared from commercially available 4-iodo-7-azaindole.[33] A mechanism for the reaction is proposed in Scheme 4.[30] The versatility of this reaction has been recently shown in the construction of related scaffolds.[34]

After optimization of the reaction conditions, the reaction was employed for the synthesis of the target BPNs **17a−m**. Compounds **16a−l** were deprotected using TFA and ethylenediamine (Scheme 3). The target compounds **18**, **19a,b**, **20a,b**, and **21** were synthesized from the corresponding amines or acids using HATU in DMF (Scheme 5)

Biological Results and Discussion. The JAK inhibitory activities of all of the target compounds are listed in Table 3. Generally, the BPNs had very good to excellent activity against the four enzymes with various selectivity profiles. Ring D substituents are important, as evidenced by the unsubstituted BPN **7a**, which showed higher potency against the four members of the JAK family when compared to BPN **7b** but lower than that of **1** with a dimethoxy substitution pattern. The dimethoxylated ring D was kept for the rest of the BPNs in the series because the docking calculations supported its importance in the solvent-exposed area. On the other hand, the side chain modifications alter both the potency and selectivity. The elongated basic side chain of BPNs **1** and **7a,b** was not optimal for the JAK inhibitory activity when compared

Scheme 5[a]

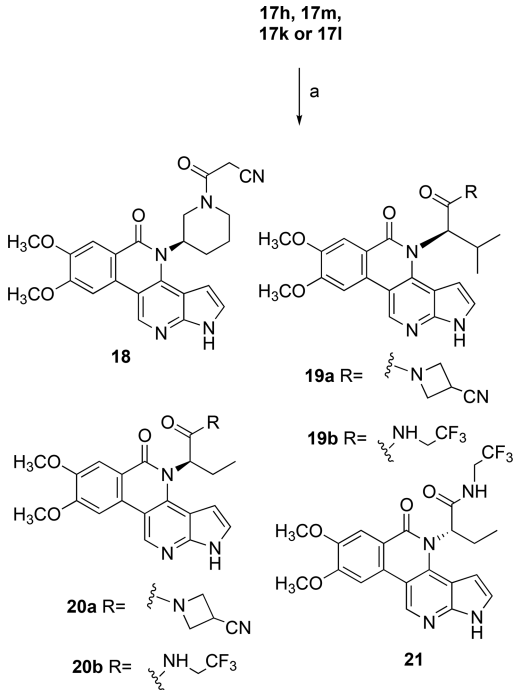

[a](a) For **18**: cyanoacetic acid, HATU, DIPEA, DMF, 21 °C, 18 h. For the rest: the appropriate amines, HATU, DIPEA, DMF, 21 °C, 18 h.

to the side chains found in **13a−c**. Additionally, BPNs **17a−d** with alicyclic side chains were among the most potent in this series with single-digit nanomolar potency against the different members of the JAK family. On the other hand, BPNs **17e−h**

DOI: 10.1021/acs.jmedchem.8b00510
J. Med. Chem. XXXX, XXX, XXX−XXX

Table 3. Janus Kinase Inhibitory Activities of the BPNs

compd	JAK1 IC_{50} (nM)	JAK2 IC_{50} (nM)	JAK3 IC_{50} (nM)	TYK2 IC_{50} (nM)
tofacitinib	1.42 ± 0.07	1.09 ± 0.17	0.24 ± 0.02	10.38 ± 0.85
1	95.62 ± 5.18	72.97 ± 2.35	129.75 ± 0.45	427.45 ± 11.45
7a	423.8 ± 4.1	229.25 ± 8.45	285.9 ± 8.5	708.65 ± 34.35
7b	3334 ± 30	489.65 ± 2.15	1111.5 ± 53.5	4766 ± 207
13a	103.15 ± 1.25	14.12 ± 0.945	9.94 ± 0.091	>1000
13b	9.89 ± 1.18	17.56 ± 0.08	6.65 ± 0.05	18.42 ± 1.05
13c	1.91 ± 0.09	10.55 ± 0.41	27.5 ± 0.75	17.4 ± 0.88
17a	4.23 ± 0.34	1.07 ± 0.05	2.92 ± 0.14	1.93 ± 0.07
17b	125.1 ± 3.6	3.57 ± 0.02	1.65 ± 0.1	39.43 ± 3.95
17c	6.59 ± 0.48	0.89 ± 0.09	1.09 ± 0.03	2.24 ± 0.30
17d	17.86 ± 0.97	1.82 ± 0.01	1.01 ± 0.026	8.38 ± 0.44
17e	37.54 ± 1.08	37.07 ± 1.55	124.1 ± 7.1	166.85 ± 36.35
17f	11.48 ± 0.61	14.70 ± 0.12	18.31 ± 0.07	32.39 ± 3.61
17g	10.61 ± 0.22	37.91 ± 2.60	143.7 ± 1.3	176.3 ± 2.3
17h	5.28 ± 0.19	8.91 ± 0.29	23.45 ± 0.11	45.10 ± 4.8
17i	58.26 ± 1.92	63.04 ± 1.69	28.94 ± 1.55	256.5 ± 16.5
17j	304.45 ± 38.05	220.8 ± 16.3	95.56 ± 1.74	1502 ± 124
18	1.20 ± 0.22	3.12 ± 0.05	2.55 ± 0.02	4.35 ± 0.38
19a	616.3 ± 20.9	1171 ± 128	818.9 ± 20.5	5730 ± 80
19b	138.1 ± 4.2	>1000	26.58 ± 0.58	1163.5 ± 3.5
20a	3.37 ± 0.13	29.6 ± 1.2	114.4 ± 0.6	73.66 ± 2.4
20b	43.78 ± 3.1	140.2 ± 7	87.03 ± 0.4	336.3 ± 12
21	30.17 ± 1.73	109.95 ± 6.1	75.03 ± 1.57	273.4 ± 2.6

with cyclic amine side chains had good to moderate activity with no characteristic selectivity profiles. Compound **18**, with an *N*-(cyanoacetyl)-3-piperidinyl side chain as found in the clinically used drug tofacitinib, also showed potent activity against the four enzymes with IC_{50} values in the low nanomolar range and low selectivity.

Compound **13a** had very interesting selectivity for JAK2 and JAK3 over JAK1 and TYK2, while **13b** was not as selective, with good activity against all four enzymes. On the other hand, BPN **13c** displayed more interesting selectivity for JAK1, with an IC_{50} value of 1.9 nM and 5-fold selectivity against JAK2 and 14-fold selectivity for JAK3. However, being an ester, BPN **13c** is expected to suffer from poor metabolic stability, and it is also racemic in nature. Compounds **19a** and **19b** were prepared to replace the ester of **17i** with amides in order to increase the stability toward metabolic hydrolysis. Unfortunately, BPN **19a** lost potency and selectivity relative to the ester **17i**, while BPN **19b** was less potent than **17i** vs JAK1, JAK2, and TYK2, but it kept very good potency and selectivity vs JAK3. Comparing the activities of the two enantiomers **17i** and **17j** indicates that the *R* configuration present in **17i** is much better than the *S* configuration.

The isopropyl group present in **19a** and **19b** was changed to an ethyl in **20a** and **20b** in order to explore effects on potency and selectivity. Compound **20a** had very good activity and selectivity vs JAK1 kinase with an IC_{50} = 3.37 nM, 10-fold selectivity vs JAK2, and 30-fold selectivity vs JAK3. Although the replacement of the ester group in **13c** with this amide side chain decreased the activity moderately, it enhanced the selectivity vs JAK1 compared to JAK2, JAK3, and TYK2. Changing the absolute configuration of the side chain of **20b** did not influence the activity very much, as shown by comparing the activities of **20b** and **21** against the four enzymes. Although **21** was consistently more active than **20b**, the configurational effect is opposite that observed with **17i** and **17j**. The trifluoroethyl amide side chain of **20b** was not as good as the cyanoazetidine ring of **20a** in enhancing the selectivity of BPN **13c**. Compound **20a** is a very good candidate for further development, with good potency and significant selectivity for JAK1 kinase.

To test the performance in a cellular context, six of the more potent compounds representing the whole series were tested for their ability to inhibit the phosphorylation of STAT-5. This assay is selective for JAK3-mediated phosphorylation of STAT-5 in SZ4 cells when activated by IL-2. Compound **18** showed the best inhibition of STAT-5 phosphorylation, with an IC_{50} value of 1.55 μM relative to tofacitinib. Compound **17a** also showed good activity with 3.72 μM IC_{50} value. On the other hand, BPNs **17b** and **17e** had very low activity. Table 4 lists the STAT-5 phosphorylation assay results.

Furthermore, the activities of BPNs **17a** and **18** were further confirmed by Western blot analyses of STAT-5 phosphorylation. Figure 5 illustrates Western blot-based determination of the IC_{50} values of STAT-5 phosphorylation for BPNs **17a** and **18**. Both compounds showed very good activity in this cell-based assay, with IC_{50} values of 65.9 and 15.3 nM, respectively, giving further evidence of the JAK3 inhibitory activity. The curves for IC_{50} determinations are provided in the Supporting Information.

The JAKs, particularly JAK3 and TYK2, are highly expressed by T cells and mediate cytokine receptor signaling.[35] A T cell proliferation assay was performed in order to access the inhibitory activities of the compounds in a functional context (Table 4 and Figure 6). The prototype JAK inhibitor tofacitinib was effective in suppressing T cell proliferation. Although not particularly active in the enzyme assays, BPN **17e**, with a methylpiperidine side chain, showed the best activity in the cellular assay with an IC_{50} value = 0.29 μM, while BPNs **17b** and **17d**, with hydrophobic side chains, had very good activity that was similar to the reference compound tofacitinib, with IC_{50} values = 0.63 and 0.76 μM, respectively. A kinome scanning assay for BPN **17b** showed some off-target

DOI: 10.1021/acs.jmedchem.8b00510
J. Med. Chem. XXXX, XXX, XXX−XXX

Table 4. Activities of Selected BPNs for Inhibition of Primary T Cell Proliferation and STAT-5 Phosphorylation in SZ4 Cells

compd	IC_{50} (μM) T cell proliferation	IC_{50} (μM) (JAK3/STAT-5) IL2/SZ4 cells[a]
tofacitinib	0.63 ± 0.26	1.21
7a	1.39 ± 0.57	NT[b]
13a	4.45 ± 2.18	NT
13b	3.97 ± 2.14	NT
13c	1.82 ± 0.9	NT
17a	0.79 ± 0.26	3.72
17b	0.63 ± 0.18	76.9
17c	3.24 ± 2.40	18.34
17d	0.76 ± 0.21	28.86
17e	0.29 ± 0.08	61.57
17f	1.45 ± 0.53	NT
17g	2.55 ± 1.48	NT
17h	1.15 ± 0.45	NT
17i	1.12 ± 0.42	NT
17j	1.67 ± 0.44	NT
18	0.68 ± 0.22	1.55
19b	5.79 ± 2.22	NT
20a	5.07 ± 2.03	NT
20b	3.66 ± 2.18	NT
21	4.66 ± 1.85	NT

[a]The numbers listed are the result of two determinations. Please see Supporting Information for the data. [b]Not tested.

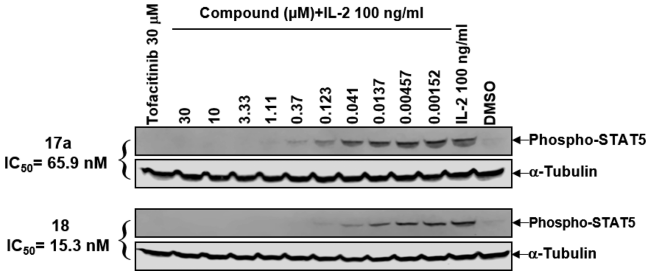

Figure 5. Western blot analysis of phospho-STAT-5 and anti-α-tubulin for BPNs **17a** and **18**.

activity, and in addition, cytotoxicity of this compound was observed in the NCI-60 cell lines (Supporting Information), which might explain the higher activity of this compound in the cell proliferation assay.

The assay results shown in Figure 6 also provide information on the cytotoxicity of the compounds to T cells. Among the compounds, **17a**, **17b**, **17d**, **17d**, and **18** displayed relatively high cell killing activity on proliferating T cells at 2 μM or lower. Moreover, eight different representative compounds were assayed for the general cytotoxicity in the NCI-60 cell line panel. Generally speaking, the BPNs were not very cytotoxic, although BPNs **1**, **7b**, **17d**, and **17i** produced negative growth percentages in a few of the cell lines when tested at a concentration of 10 μM. The results are listed in Table 1s in Supporting Information. Twelve BPNs were tested for their Top1 inhibitory activity, and none of them displayed significant activity. Figures 1s, 2s, and 3s in the Supporting Information show the DNA fragmentation patterns produced by the 12 compounds.

On the other hand, BPNs **7a** and **17f–j** displayed good activity when compared to tofacitinib (Table 4 and Figure 6). In addition, BPNs **13a**, **13b**, **17c**, **19b**, **20a**, **20b**, and **21** had

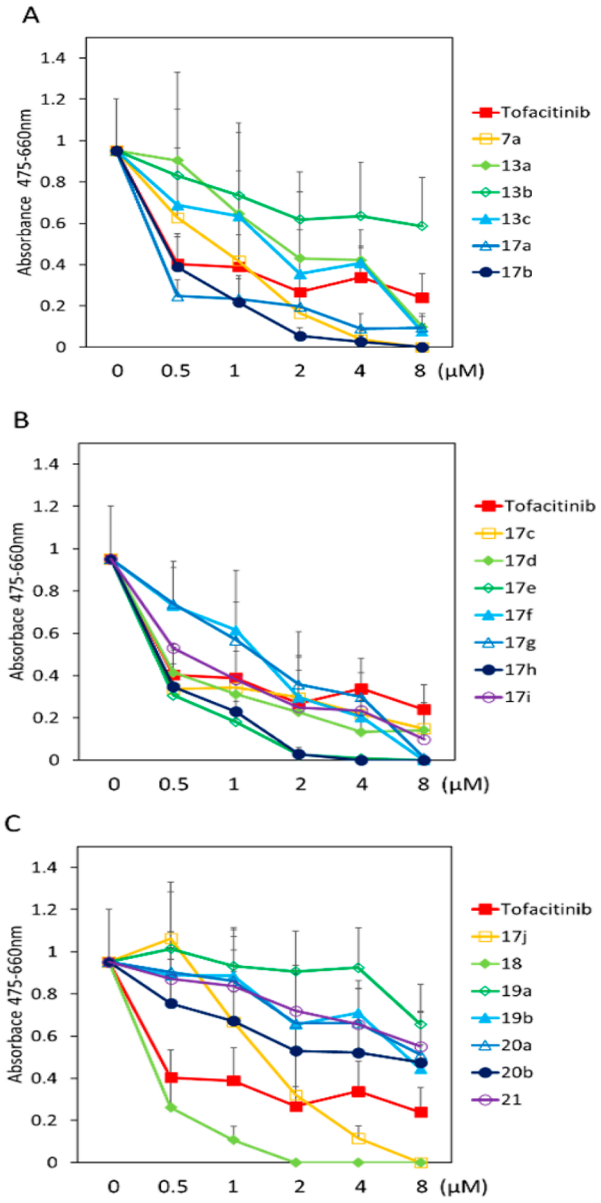

Figure 6. Effects of BPNs on proliferation of primary murine T cells. Naive $CD4^+$ T cells were isolated from mouse spleens and cultured with the indicated BPNs in the presence of T cell activators (antibodies to CD3 and CD28) and IL-2 for 3 days. T cell proliferation was assessed by XTT staining and measured at 475 nm with a microplate reader (SpectraMax i3X, Molecular Devices). The assay was repeated three times (n = 3 for each dose and inhibitor), and mean ± SEM ranges are shown.

moderate inhibitory activity on T cell proliferation when compared to tofacitinib, with IC_{50} values higher than 3 μM. The absence of a good correlation between the cellular and enzyme inhibition data may be due to the differential expression of various JAK subtypes in T cells. In addition, the physicochemical properties of the BPNs and differences in cell permeability may also play a major role in the cellular activities as will be discussed shortly.[36]

Cytokines such as IFNγ and IL-17 play key roles in mediating the inflammatory activities of T cells. These two cytokines are produced by distinct T cell subsets that are antagonistic to each other.[37] The effects of selected JAK inhibitors on T cell expression of IFNγ and IL-17 were

DOI: 10.1021/acs.jmedchem.8b00510
J. Med. Chem. XXXX, XXX, XXX−XXX

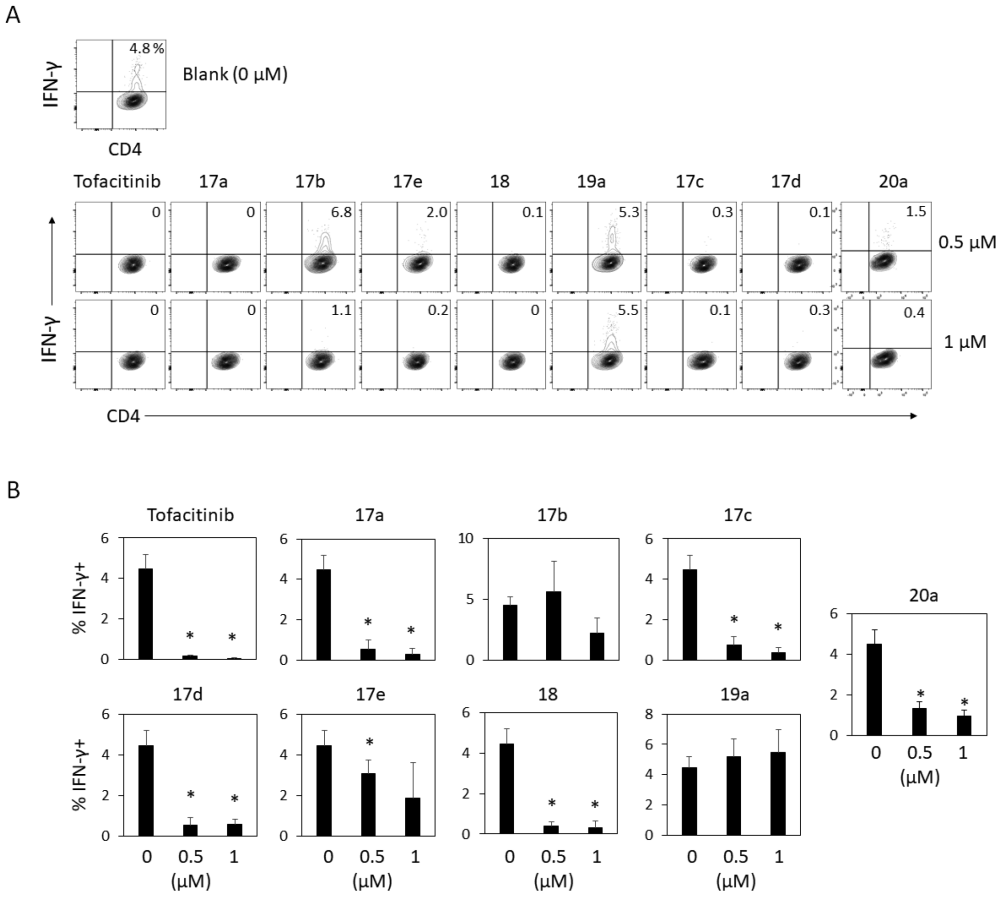

Figure 7. Effects of compounds on IFNγ expression by primary murine T cells. Naïve $CD4^+$ T cells were isolated from mouse spleens and cultured with the indicated compounds in the presence of T cell activators (antibodies to CD3 and CD28) and IL-2 for 5 days. (A) T cell expression of IFNγ was assessed by intracellular staining of activated T cells with an antibody to IFNγ. The cells were analyzed with a Canto II flow cytometer (Becton Dickinson). (B) % IFNγ expression by T cells in the presence of test compounds compared to control. Note that data for **17b** and **19a** are presented with different scales on the *y*-axes of the bar graphs than the other compounds. The assay was repeated three times ($n = 3$ for each dose and inhibitor), and mean ± SEM are shown in part B. *Significant differences from controls (no inhibitor) by Student *t* test (paired one-tailed).

examined. Tofacitinib was effective in suppressing IFNγ production (Figure 7). The BPNs **17a**, **17c**, **17d**, **18**, and **20a** were also similarly effective in suppressing IFNγ production. In general, there is an inverse relationship between IFNγ and IL-17 production because the IFNγ produced by T cells effectively suppresses IL-17 production. There is much greater T cell production of IL-17 in the presence of tofacitinib (Figure 8). Similarly, IL-17 production was increased in the presence of **17a**–**e**, **18**, and **20a**, but it was not increased significantly by **19a** as expected from the data reported in Figure 7. These results indicate that in general the compounds have potent modulatory activity on the production of T cell effector cytokines.

The results from the assays for T cell proliferation and cytokine production are generally in line with those expected from the JAK inhibition assay. However, the most potent compounds in the isolated enzyme assay were not necessarily the most potent ones in suppressing T cells. This may be because the compounds need to have additional characteristics such as membrane permeability and metabolic stability to be effective as inhibitors within cells. Also, the differences among the compounds on target or cytokine signaling selectivity can account for such differences among the assays. For example, IL-2 and IL-23 drive T cell proliferation in the assays that were used. IL-2 uses JAK1 and JAK3, whereas IL-23 uses JAK2 and TYK2. If a compound inhibits JAK2 but not JAK1 or JAK3, it would not effectively inhibit IL-2-driven T cell proliferation. Thus, the results from the biochemical inhibition assays would not exactly match the results from cell-based assays or in vivo experiments.

Kinome Selectivity. For any new kinase inhibitor scaffold, it is always important to show selectivity against the target of interest to avoid possible side effects and toxicity.[38,39] To investigate the kinome selectivity of the new BPN scaffold, three potent BPNs were tested for their abilities to inhibit various members of the human kinome (468 kinases) (KINOMEscan Assay Platform by DiscoverX). Compounds **17b**, **18**, and **20a** were assayed for their ability to displace an immobilized ATP binding site ligand from 403 normal kinases and 65 mutant kinases (Figure 9). These compounds demonstrated excellent selectivity profiles. Table 5 shows the selectivity scores and number of hits for the three compounds tested. The selectivity score or S-score is a quantitative measure of compound selectivity. It is calculated by dividing the number of enzyme hits to by the total number of distinct kinases tested, excluding mutant variants. This value can be calculated using %Ctrl as a potency threshold and provides a quantitative method of describing compound selectivity to facilitate comparison of different compounds.

DOI: 10.1021/acs.jmedchem.8b00510
J. Med. Chem. XXXX, XXX, XXX−XXX

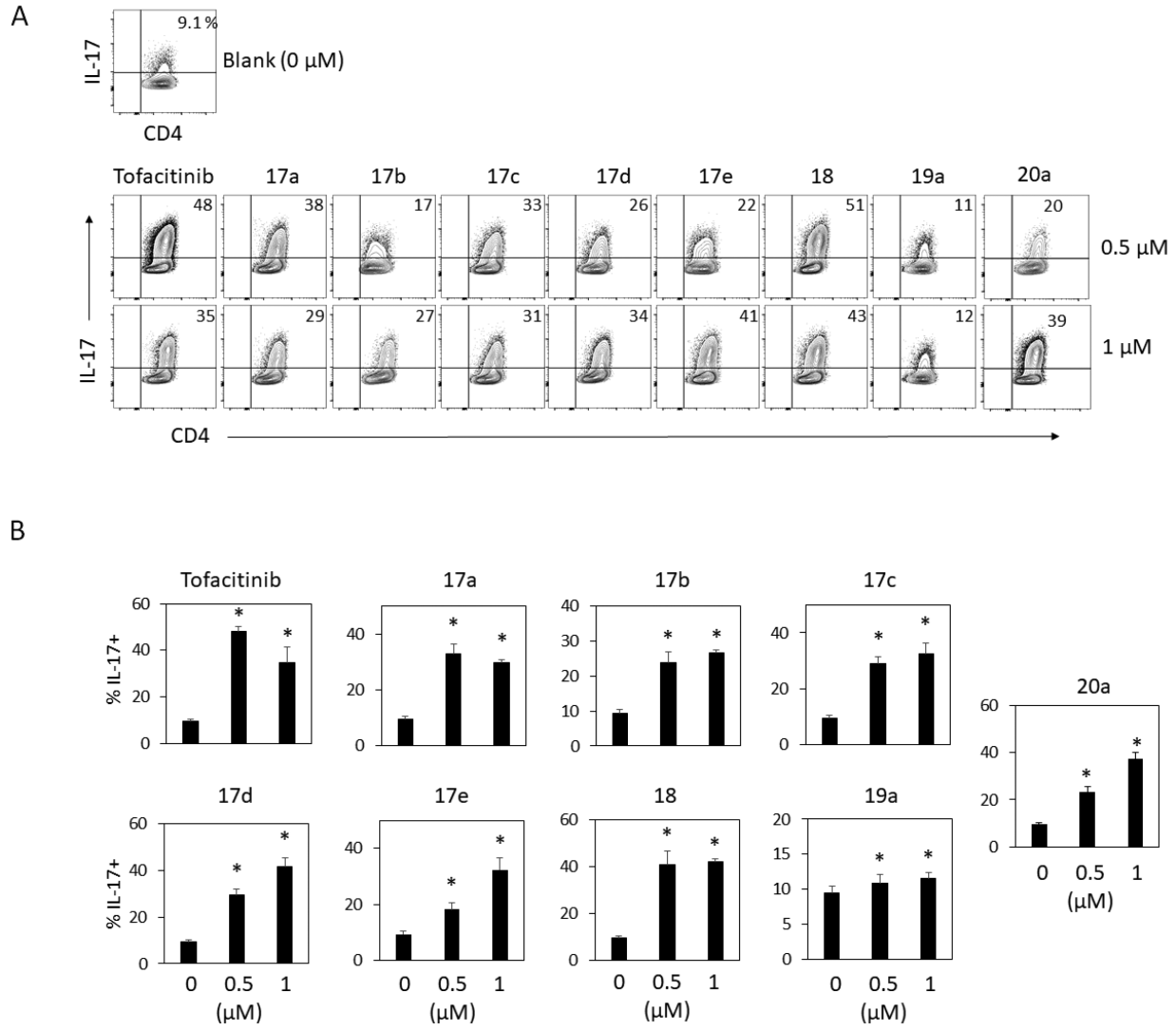

Figure 8. Effects of compounds on IL-17 expression by primary murine T cells. Naïve $CD4^+$ T cells were isolated from mouse spleens and cultured with the indicated compounds in the presence of T cell activators (antibodies to CD3 and CD28) and the cytokines listed in the method section for 5 days. (A) T cell expression of IL-17 was assessed by intracellular staining of activated T cells with an antibody to IL-17. The cells were analyzed with a Canto II flow cytometer. (B) Percent IL-17 expression by CD4 T cells in the presence of test compounds compared to control. Note the differing scales on the *y*-axes of the bar graphs. The assay was repeated three times ($n = 3$ for each dose and inhibitor), and mean ± SEM are shown in part B. *Significant differences from controls (no inhibitor) by Student *t* test (paired one-tailed).

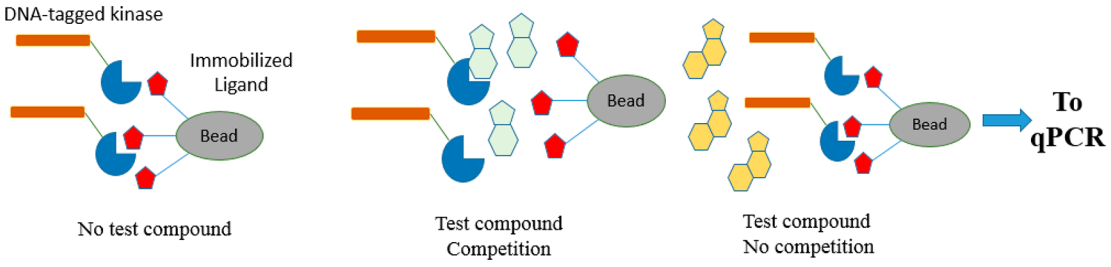

Figure 9. Technique used for determination of kinome selectivity.

BPN **20a** had outstanding selectivity for the four Janus kinases (Supporting Information, Figure 4s), and of those, it was most active vs JAK-1 (Table 3). BPNs **17b** and **18** affected some additional kinases in the kinome in a potent manner. Table 6 lists the K_d values in nM for some of the additional kinases affected by **17b** and **18**. Both of them bound to BIKE kinase in the low nanomolar range. Compound **17b** also showed good binding activity to FLT3(N841I), SNARK, and TrkA[40] in the low nanomolar range, and it had moderate binding to Ark5. Compound **18** demonstrated potent inhibition of YSK4 kinase. A complete list of kinases tested and the kinome maps are available in Table 2s and Figure 4s in the Supporting Information.

ADME Properties. To evaluate the preliminary ADME properties of this new BPN class of JAK inhibitors, five different compounds were tested for solubility, cell perme-

DOI: 10.1021/acs.jmedchem.8b00510
J. Med. Chem. XXXX, XXX, XXX−XXX

Table 5. Kinome Selectivity Scores of BPNs 17b, 17d, and 18

compd	selectivity score type	no. of enzyme hits	no. of nonmutant kinases	screening concentration (nM)	selectivity score[a]
17b	S(35)	24	403	100	0.06[b]
17b	S(10)	6	403	100	0.015[c]
17b	S(1)	0	403	100	0[d]
18	S(35)	40	403	100	0.099
18	S(10)	9	403	100	0.022
18	S(1)	5	403	100	0.012
20a	S(35)	4	403	100	0.01
20a	S(10)	0	403	100	0
20a	S(1)	0	403	100	0

[a]The numbers reflect the abilities of the test compounds to inhibit the binding of the kinases to an immobilized ATP binding site ligand. Lower numbers indicate higher selectivities of the test compounds for the enzymes. [b](Number of nonmutant kinases with %Ctrl <35)/(number of nonmutant kinases tested) where %Ctrl is the percentage of enzymes remaining bound to an immobilized ATP binding site ligand in the presence of 100 nM concentration of the test compound. [c](Number of nonmutant kinases with %Ctrl <10)/(number of nonmutant kinases tested). [d](Number of nonmutant kinases with % Ctrl <1)/(number of nonmutant kinases tested).

Table 6. K_d (nM) Values for Kinases Identified as Hits During Kinome Scanning

kinase	17b	18
ARK5	42	NT[a]
BIKE	7.5	0.22
FLT3(D835V)	NT	>100
FLT3(N841I)	15	NT
SNARK	3.5	NT
TRKA	2.3	NT
YSK4	NT	1.2

[a]NT: Not tested.

ability, and liver microsomal metabolic stability. Table 7 lists the results for BPNs **17a**, **17b**, **17e**, **18**, and **20a**. Most of them had low aqueous solubilities (PBS buffer, pH 7.4) with the exception of compound **17e**, which has a methylpiperidine side chain that is well-known to enhance the solubility. In contrast, with the exception of **17e**, the compounds displayed enhanced solubilities in gastric and intestinal fluids relative to the PBS buffered media. The Caco-2 cellular permeability profiles of these particular BPNs are relatively unfavorable, with BPNs **17e** and **18** being potential substrates for active efflux transport. On the other hand, three of the BPNs (**17e**, **18**, and **20a**) had excellent metabolic stabilities against human liver microsomal enzymes with $t_{1/2}$ values over 60 min.

Molecular Modeling. The structures of the inhibitors were docked in the ATP binding sites of the four subtypes of the JAK family. Compounds **17b**, **17d**, and **18** were the most active against the JAK3 enzyme, with IC_{50} values of 1.65, 1.01, and 2.55 nM, respectively, while BPNs **13c**, **18**, and **20a** were the most active against JAK1 with IC_{50} values of 1.91, 1.20, and 3.37 nM, respectively. Figure 10 illustrates a comparison between the binding modes of compound **17d** in the ATP binding sites of JAK1 and JAK3. As expected, the pyrrolopyridine part in all of the compounds made the essential hinge binding interactions with Leu-905 and Glu-903 in JAK3 and with Leu-959 and Glu-957 in JAK1 involved in the formation of hydrogen bonds.

There is only a minor difference between the structures of the JAK1 and JAK3 ATP binding sites in the activation loop (green) (glycine vs alanine). This can partially explain the difference in the activity between compound **17d** against JAK1 (IC_{50} = 17.86 nM) and JAK3 (IC_{50} = 1.01 nM).

On the other hand, BPN **18** had excellent inhibitory activity against both enzymes with very good cellular potency and kinome selectivity. The hypothetical binding modes of BPN **18** with JAK1 and JAK3 are illustrated in Figure 11. Compound **18** was calculated to have a hydrophobic interaction with the activation loop (colored green) in both enzymes, but the hydrophobic part of the piperidine side chain is not large enough to cause a significant difference in activity between the two enzymes (Table 3). The cyanoacetate side chain is directed toward the phosphate binding loop in both enzymes (colored red in Figure 11), which is a relatively hydrophilic region that plays a role in the potency of this compound.

Finally, compound **20a** was not very active in the T cell proliferation assay. This can be explained by its good selectivity against JAK1, which is moderately expressed in the cells that were used in the assay, in addition to poor cellular permeability. A clear explanation for the JAK1 selectivity of **20a** could not be drawn from the molecular modeling, but it can be hypothesized that the nonbonded interaction of the ethyl side chain with the activation loop in JAK1 and JAK3 may contribute to the difference in activity. The presence of the larger Ala966 moiety in JAK3 relative to the Gly1020 residue of JAK1 can limit the free movement of the ethyl group in the hydrophobic pocket of the activation loop while the smaller glycine residue can accommodate the ethyl side chain of **20a** as shown in Figure 12.

Table 7. Preliminary ADME Properties of Selected Compounds

compd	aqueous solubility (PBS, pH 7.4) (μM)	aqueous solubility (simulated intestinal fluid) (μM)	aqueous solubility (simulated gastric fluid) (μM)	A−B permeability (Caco-2, pH 6.5/7.4) permeability (10^{-6} cm/s)	B−A permeability (Caco-2, pH 6.5/7.4) permeability (10^{-6} cm/s)	human liver microsomes ($t_{1/2}$) (min)
17a	NS[a]	12.5	NS	NP[c]	NP	17
17b	1.7	8.8	60.7	2.9	0.1	7
17e	195.8	200	198.1	0.4	43.4	>60
18	NS	NS	187.3	0.3	9.6	>60
20a	13.6	192.9	24.2	0.1	14	>60
tamoxifen	2	NT	NT	NT	NT	NT
ranitidine	NT[b]	NT	NT	0.3	2	NT
propranolol	NT	NT	NT	33.5	36.7	>60

[a]NS: Not soluble. [b]NT: Not tested. [c]NP: Not permeable.

DOI: 10.1021/acs.jmedchem.8b00510
J. Med. Chem. XXXX, XXX, XXX−XXX

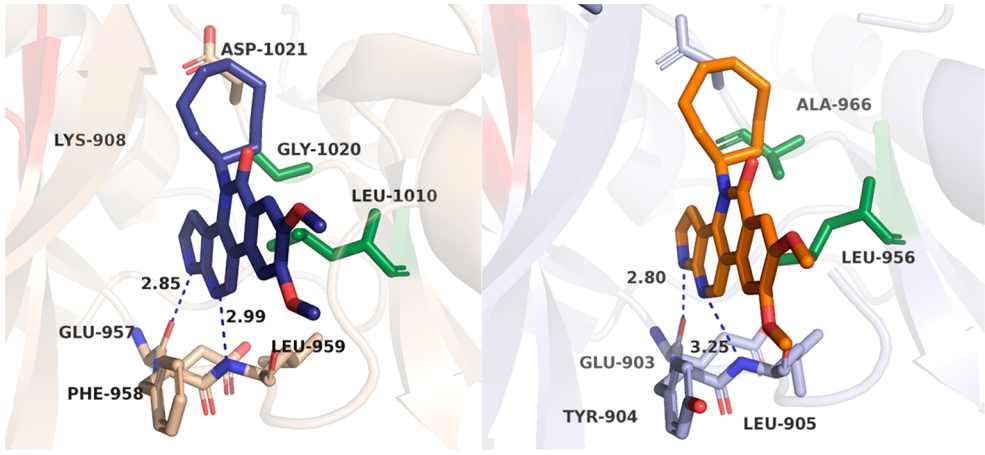

Figure 10. Hypothetical binding modes of compound **17d** in JAK1 (left) (PDB 4I5C) and JAK3 (right) (PDB 3LXK).

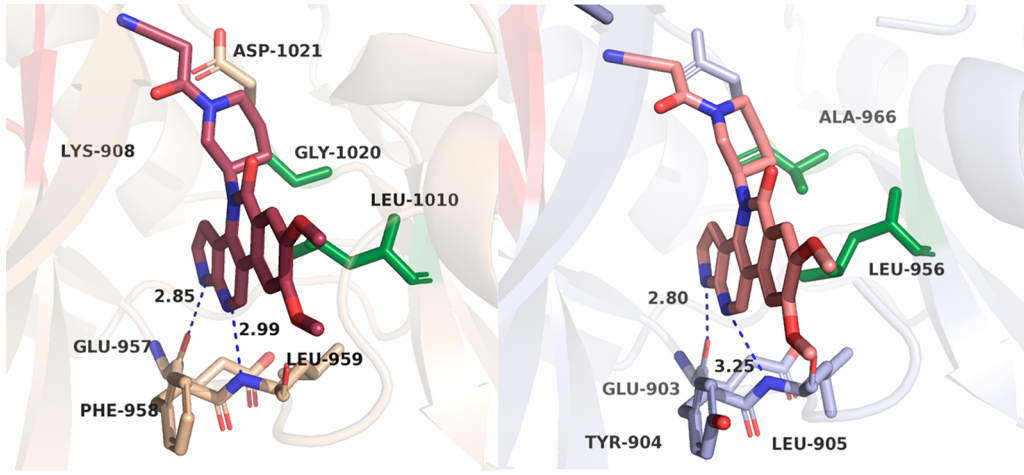

Figure 11. Hypothetical binding mode of compound **18** in JAK1 (left) (PDB 4I5C) and JAK3 (right) (PDB 3LXK).

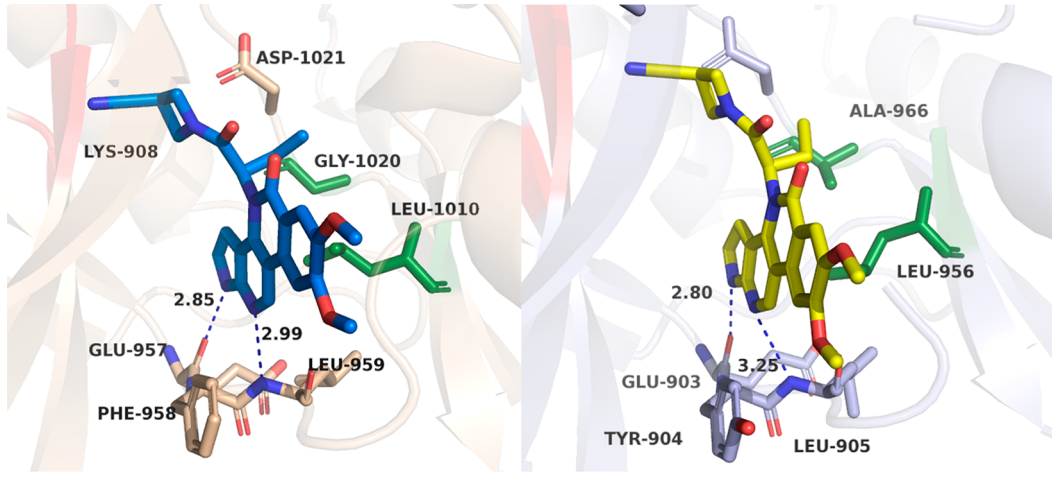

Figure 12. Hypothetical binding mode of **20a** in JAK1 l (left) (PDB 4I5C) and JAK3 (right) (PDB 3LXK).

Determination of Anti-Inflammatory Activity in a Mouse Model. To access anti-inflammatory activity in vivo, compound **17b**, tofacitinib, or vehicle (in 10% DMSO and 10% Cremophor EL) were each administered to groups of seven mice two months after collagen-induced inflammation, and the activity was measured on each paw using a standard 0−4 rheumatoid arthritis scale. This approach is more realistic than the usual collagen-induced rheumatoid arthritis studies because it measures the ability of the drugs to treat existing inflammation rather than prevent it. The total scores, which reflect the degree of inflammation and ankylosis, are plotted as a function of time (Figure 13). The *t* test reveals that both tofacitinib and **17b** cause a significantly different response

DOI: 10.1021/acs.jmedchem.8b00510
J. Med. Chem. XXXX, XXX, XXX−XXX

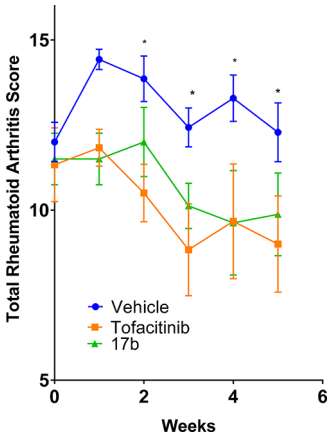

Figure 13. Mean rheumatoid arthritis score. Mouse paw collagen-induced inflammation assay (male DBA-1 $n = 7$) of compound **17b**. Daily doses of tofacitinib or **17b** were administered subcutaneously in 10% DMSO and 10% Cremophor EL to seven mice. Paw inflammation for each paw was expressed on a 0−4 mean rheumatoid arthritis scale. The t test revealed that both tofacitinib and **17b** caused a significantly different response compared to the vehicle control and that there is not a statistically significant difference between the two drugs. The calculated P values were 0.0481 for week 2, 0.0443 for week 3, 0.0442 for week 4, and 0.0473 for week 5.

compared to the vehicle control and that there is not a statistically significant difference between the two drugs.

CONCLUSION

A novel tetracyclic BPN series of JAK inhibitors was discovered by the hybridization of Chk1 inhibitors and Top1 poisons. The new series showed interesting enzymatic activity profiles against the four members of the JAK family with potencies in the low nanomolar range and variable selectivities. Cellular kinase and T-cell proliferation assays revealed promising activity of the new scaffold compared to the clinically used drug tofacitinib. Preliminary testing of the ADME properties of a limited number of compounds in this new class indicated that several of them suffer from low aqueous solubility and poor cellular permeability that might be improved by fine-tuning the side chain. In vivo studies in a mouse rheumatoid arthritis model revealed BPN **17a** has anti-inflammatory activity that is comparable to that of the clinically used drug tofacitinib. Molecular modeling was used to show the hypothetical JAK1 and JAK3 binding modes of some of the more potent compounds in this class.

EXPERIMENTAL SECTION

General. Melting points were determined with a Mel-Temp apparatus using capillary tubes and are uncorrected. The proton nuclear magnetic resonance spectra (^{1}H NMR) were recorded using Bruker ARX300 300 MHz or Bruker DRX500 500 MHz spectrometers. IR spectra were obtained with a PerkinElmer 1600 series FTIR spectrometer. For biologically tested compounds, the HPLC major peak accounted for ≥95% of the combined total peak area when monitored by a UV detector at 254 nm. HPLC analyses were performed on a Waters 1525 binary HPLC pump/Waters 2487 dual λ absorbance detector system. Analytical thin-layer chromatography was conducted on Baker-flex silica gel IB2-F plates, and compounds were visualized with UV light at 254 nm. Silica gel flash chromatography was performed using 230−400 mesh silica gel.

4-(3-(Dimethylamino)propyl)-7,8-dimethoxy-1,4-dihydro-5*H*-benzo[*c*]pyrrolo[2,3-*h*][1,6]naphthyridin-5-one (1). Compound **6b** (0.05 g, 0.13 mmol) was dissolved in THF (10 mL), and concd HCl (2 mL) was added to the solution. The mixture was heated at 80 °C for 18 h and then cooled to room temperature. The THF was evaporated under reduced pressure, and the residue was treated with saturated aq $NaHCO_3$ solution until the effervescence ceased. The mixture was extracted with $CHCl_3$ (3 × 15 mL), and the combined organic layer was washed with water (2 × 10 mL) and brine (1 × 15 mL), dried with sodium sulfate, and evaporated to give a light-brown residue. The residue was purified by silica gel column chromatography using $CHCl_3$−MeOH (8.5:1.5) to give the final compound **1** as a light-brown foam (26 mg, 59%). ^{1}H NMR (300 MHz, DMSO-d_6) δ 12.11 (s, 1 H), 9.40 (s, 1 H), 8.04 (s, 1 H), 7.73 (s, 1 H), 7.55 (s, 1 H), 6.93 (s, 1 H), 4.69−4.62 (m, 2 H), 4.05 (s, 3 H), 3.91 (s, 3 H), 2.63−2.48 (m, 2 H), 2.26 (s, 6 H), 2.12−1.94 (m, 2 H). MALDIMS m/z 381 $(MH)^+$. HRESIMS calcd for $C_{21}H_{25}N_4O_3$ $(MH)^+$ 381.1927, found 381.1920. C18 HPLC purity: 100% (MeOH−H_2O, 85:15).

4-Bromo-1-(methoxymethyl)-1*H*-pyrrolo[2,3-*b*]pyridine (3). This compound was prepared according to a published literature procedure[28] and isolated as yellow oil (1.16 g, 96%). ^{1}H NMR (300 MHz, $CDCl_3$) δ 8.15 (d, J = 5.2 Hz, 1 H), 7.40 (d, J = 3.6 Hz, 1 H), 7.31 (d, J = 5.2 Hz, 1 H), 6.59 (d, J = 3.6 Hz, 1 H), 5.64 (s, 2 H), 3.30 (s, 3 H).

***N*^{1}-(1-(Methoxymethyl)-1*H*-pyrrolo[2,3-*b*]pyridin-4-yl)-*N*^{3},*N*^{3}-dimethylpropane-1,3-diamine (4).** Compound **3** (1 equiv, 0.5 g, 2.01 mmol), N^1,N^1-dimethylpropane-1,3-diamine (0.275 g, 2.7 mol, 1.3 equiv), $Pd_2(dba)_3$ (95 mg, 5 mol %), xantphos (120 mg, 10 mol %), and cesium carbonate (1.35 g, 4.15 mmol, 2 equiv) were mixed in a 45 mL pressure tube, and anhydrous dioxane (15 mL) was added to the mixture. Argon was bubbled through the reaction mixture for 2 min, and then the pressure tube was capped and placed directly in a preheated oil bath at 110 °C. The mixture was heated for 16 h and then allowed to cool to room temperature. $CHCl_3$ (20 mL) was added to the mixture and then it was filtered through a bed of Celite and the residue left on the filter pad was washed with additional $CHCl_3$ (20 mL). The filtrate was evaporated to afford a dark residue that was purified by silica gel column chromatography using a $CHCl_3$−MeOH mixture (9:1) as the eluent to provide the amine **4** as a light-brown oil (0.4 g, 74%). ^{1}H NMR (300 MHz, $CDCl_3$) δ 8.06 (d, J = 5.5 Hz, 1 H), 7.08−7.02 (m, 1 H), 6.50 (d, J = 3.6 Hz, 1 H), 6.25 (s, 1 H), 6.19 (d, J = 5.6 Hz, 1 H), 5.57 (s, 2 H), 3.51−3.45 (m, 2 H), 3.29 (s, 3 H), 2.73 (t, J = 6.3 Hz, 2 H), 2.48 (s, 6 H), 2.07−1.87 (m, 2 H). HRESIMS m/z calcd for $C_{14}H_{22}N_4O$ $(MH)^+$ 263.1866, found 263.1869.

General Procedure for the Preparation of the Amides 5a−c. The appropriate benzoyl chloride derivative was prepared by heating the necessary 2-bromobenzoic acid derivative (0.9 mmol, 1 equiv) and thionyl chloride (5 mL) at reflux for 2 h, followed by removal of excess thionyl chloride under vacuum. The acid chloride (1 equiv, 0.9 mmol) in anhydrous DCM (5 mL) was added dropwise to an ice-cold solution of the amine **4** (0.25 g, 1 equiv, 0.9 mmol) and TEA (10 equiv) in anhydrous DCM (20 mL). The mixture was heated at reflux for 5 h. After cooling to room temperature, the mixture was washed with saturated $NaHCO_3$ solution (1 × 20 mL), water (2 × 20 mL), and brine (1 × 20 mL) and dried with anhydrous sodium sulfate. The residue obtained after the evaporation of DCM was subjected to silica gel column chromatography using $CHCl_3$−MeOH as eluent to yield the desired amides **5a−c**.

*N-(3-(Dimethylamino)propyl)-2-bromo-N-(1-(methoxymethyl)-1H-pyrrolo[2,3-b]pyridin-4-yl)benzamide (**5a**).* This compound was isolated as a brown gum (0.27 g, 57%). ^{1}H NMR (300 MHz, $CDCl_3$) δ 8.16−8.08 (m, 1 H), 7.72−7.66 (m, 1 H), 7.38 (d, J = 3.6 Hz, 1 H), 6.91−6.85 (m, 4 H), 6.68−6.61 (m, 1 H), 5.59 (s, 2 H), 4.15−4.09 (m, 2 H), 3.27 (s, 3 H), 2.54−2.48 (m, 2 H), 2.26 (s, 6 H), 1.94−1.88 (m, 2 H). HRESIMS m/z calcd for $C_{21}H_{25}BrN_4O_2$ $(MH)^+$ 445.1234/447.1216, found 445.1231/447.1215.

*2-Bromo-N-(3-(dimethylamino)propyl)-4,5-dimethoxy-N-(1-(methoxymethyl)-1H-pyrrolo[2,3-b]pyridin-4-yl)benzamide (**5b**).* This compound was isolated as a dark-brown gum (0.26 g, 54%). ^{1}H NMR (300 MHz, $CDCl_3$) δ 8.16 (s, 1 H), 7.38 (d, J = 3.6 Hz, 1 H), 6.91 (s, 1 H), 6.82 (s, 1 H), 6.62 (d, J = 3.6 Hz, 1 H), 6.47 (s, 1 H), 5.59 (s, 2

DOI: 10.1021/acs.jmedchem.8b00510
J. Med. Chem. XXXX, XXX, XXX−XXX

H), 4.11−4.04 (m, 2 H), 3.75 (s, 3 H), 3.40 (s, 3 H), 3.26 (s, 3 H), 2.64−2.59 (m, 2 H), 2.31 (s, 6 H), 1.97−1.89 (m, 2 H). HRESIMS m/z calcd for $C_{23}H_{29}BrN_4O_4$ $(MH)^+$ 505.1444/507.1427, found 505.1442/507.1423.

*2-Bromo-N-(3-(dimethylamino)propyl)-N-(1-(methoxymethyl)-1H-pyrrolo[2,3-b]pyridin-4-yl)-5-nitrobenzamide (**5c**).* This compound was isolated as a dark-brown gum (0.35 g, 74%). ^{1}H NMR (300 MHz, $CDCl_3$) δ 8.15 (d, J = 5.0 Hz, 1 H), 7.86 (s, 1 H), 7.80 (dd, J = 8.7, 2.6 Hz, 1 H), 7.56 (d, J = 8.7 Hz, 1 H), 7.43 (d, J = 3.6 Hz, 1 H), 6.96 (d, J = 5.1 Hz, 1 H), 6.64 (d, J = 3.7 Hz, 1 H), 5.57 (s, 2 H), 4.12 (s, 2 H), 3.22 (s, 3 H), 2.54 (s, 2 H), 2.30 (s, 6 H), 2.02−1.86 (m, 2 H). HRESIMS m/z calcd for $C_{21}H_{24}BrN_5O_4$ $(MH)^+$ 490.1084/492.1067, found 490.1085/492.1070.

General Procedure for the Direct Intramolecular Arylation Reaction to Afford 6a−c. The benzamides **5a−c** (1 equiv, 0.5 mmol) were dissolved in DMA (5 mL), and $Pd(OAc)_2$ (10 mol %), Cs_2CO_3 (2 equiv), Ag_2CO_3 (2 equiv), and $PCy_3{\cdot}HBF_4$ (20 mol %) were added. The reaction mixture was heated at 130 °C under Ar atmosphere for 18 h. The reaction mixture was cooled to room temperature, and EtOAc (10 mL) was then added. The mixture was filtered through a bed of Celite, and the residue left on the filter pad was washed with EtOAc (about 20 mL). The filtrate was transferred to a separatory funnel and washed with water several times (5 × 15 mL) to remove the DMA and brine (1 × 15 mL). The organic layer was dried and evaporated, and the residue was purified with column chromatography using $CHCl_3$−MeOH (9:1) as the eluent to give the tetracyclic compounds **6a−c**.

*4-(3-(Dimethylamino)propyl)-1-(methoxymethyl)-1,4-dihydro-5H-benzo[c]pyrrolo[2,3-h][1,6]naphthyridin-5-one (**6a**).* This compound was isolated as a brown semisolid (0.06 g, 32%). ^{1}H NMR (300 MHz, $CDCl_3$) δ 9.31 (s, 1 H), 8.53 (d, J = 8.1 Hz, 1 H), 8.39 (d, J = 8.2 Hz, 1 H), 7.80 (t, J = 7.7 Hz, 1 H), 7.57 (t, J = 7.6 Hz, 1 H), 7.42 (d, J = 3.8 Hz, 1 H), 7.02 (d, J = 3.8 Hz, 1 H), 5.73 (s, 2 H), 4.82−4.73 (m, 2 H), 3.36 (s, 3 H), 2.73 (t, J = 7.2 Hz, 2 H), 2.42 (s, 6 H), 2.29−2.21 (m, 4 H). HRESIMS m/z calcd for $C_{21}H_{24}N_4O_2$ $(MH)^+$ 365.1972, found 365.1970.

*4-(3-(Dimethylamino)propyl)-7,8-dimethoxy-1-(methoxymethyl)-1,4-dihydro-5H-benzo[c]pyrrolo[2,3-h][1,6]naphthyridin-5-one (**6b**).* This compound was isolated as a light-brown oil (0.06 g, 28%). ^{1}H NMR (300 MHz, $CDCl_3$) δ 9.19 (s, 1 H), 7.89 (s, 1 H), 7.71 (s, 1 H), 7.41 (d, J = 3.8 Hz, 1 H), 6.99 (d, J = 3.8 Hz, 1 H), 5.73 (s, 2 H), 4.78 (s, 2 H), 4.10 (s, 3 H), 4.04 (s, 3 H), 3.38−3.31 (m, 2 H), 2.81−2.75 (m, 2 H), 2.45 (s, 6 H), 2.30−2.24 (m, 2 H). HRESIMS m/z calcd for $C_{23}H_{28}BrN_4O_4$ $(MH)^+$ 425.2183, found 425.2187.

*4-(3-(Dimethylamino)propyl)-1-(methoxymethyl)-7-nitro-1,4-dihydro-5H-benzo[c]pyrrolo[2,3-h][1,6]naphthyridin-5-one (**6c**).* This compound was isolated as a yellow solid (0.03 g, 14%): mp 125−127 °C. ^{1}H NMR (300 MHz, $CDCl_3$) δ 9.17 (d, J = 2.5 Hz, 1 H), 8.24 (d, J = 5.6 Hz, 1 H), 8.19 (dd, J = 8.8, 2.5 Hz, 1 H), 7.76 (s, 1 H), 7.71 (d, J = 8.8 Hz, 1 H), 6.80 (d, J = 5.8 Hz, 1 H), 5.66 (s, 2 H), 4.21−4.15 (m, 2 H), 3.37 (s, 3 H), 2.61 (s, 2 H), 2.41 (s, 6 H), 2.11−2.05 (m, 2 H). HRESIMS m/z calcd for $C_{21}H_{23}BrN_5O_4$ $(MH)^+$ 410.1823, found 410.1820.

4-(3-(Dimethylamino)propyl)-1,4-dihydro-5*H*-benzo[*c*]-pyrrolo[2,3-*h*][1,6]naphthyridin-5-one (7a). This compound was prepared from **6a** following the same procedure as for **1** and isolated as a dark-brown solid (0.026 g, 58%): mp 185−187 °C. IR (thin film) 2950, 1648, 1578, 1418, 1338, 1314, 1036 cm^{-1}. ^{1}H NMR (300 MHz, DMSO-d_6) δ 12.16 (s, 1 H), 9.38 (s, 1 H), 8.68 (d, J = 8.1 Hz, 1 H), 8.36 (d, J = 8.0 Hz, 1 H), 7.85 (t, J = 7.6 Hz, 1 H), 7.66−7.47 (m, 2 H), 6.99−6.92 (m, 1 H), 4.74−4.59 (m, 2 H), 2.66 (s, 2 H), 2.33 (s, 6 H), 2.08−1.99 (m, 2 H). MALDIMS m/z 321 $(MH)^+$. HRESIMS calcd for $C_{19}H_{21}N_4O$ $(MH)^+$ 321.1716, found 321.1709. C18 HPLC purity: 99.65% (MeOH−H_2O, 85:15).

4-(3-(Dimethylamino)propyl)-7-nitro-1,4-dihydro-5*H*-benzo[*c*]pyrrolo[2,3-*h*][1,6]naphthyridin-5-one (7b). This compound was prepared from **6c** following the same procedures as for **1** and isolated as a yellow powder (0.032 g, 71%): mp 205−207 °C. IR (thin film) 2864, 1667, 1611, 1572, 1519, 1491, 1433, 1403, 1328, 1135, 1077 cm^{-1}. ^{1}H NMR (300 MHz, DMSO-d_6) δ 12.35 (s, 1 H), 9.44 (s, 1 H), 9.04 (d, J = 2.6 Hz, 1 H), 8.93 (d, J = 9.2 Hz, 1 H), 8.54 (dd, J = 9.0, 2.6 Hz, 1 H), 7.64 (s, 1 H), 7.01 (s, 1 H), 4.69−4.62 (m, 2 H), 2.55−2.50 (m, 2 H), 2.24 (s, 6 H), 2.05−1.96 (m, 3 H). ^{13}C NMR (126 MHz, DMSO) δ 160.94, 150.55, 145.81, 142.17, 139.52, 139.02, 126.94, 125.93, 124.06, 123.93, 123.42, 106.36, 106.02, 102.34, 56.60, 45.50, 43.52, 26.06. MALDIMS m/z 366 $(MH)^+$. HRESIMS calcd for $C_{19}H_{20}N_5O_3$ $(MH)^+$ 366.1566, found 366.1560. C18 HPLC purity: 100% (MeOH−H_2O, 85:15).

1-((2-(Trimethylsilyl)ethoxy)methyl)-1*H*-pyrrolo[2,3-*b*]-pyridin-4-amine (9). SEM-protected 4-bromo-7-azaindole **8** (2 g, 8.3 mmol) was added to a mixture of xantphos (0.48 g, 0.83 mmol), $Pd(OAc)_2$ (0.093 g, 0.41 mmol), benzophenone imine (1.8 g, 9.93 mmol), and Cs_2CO_3 (5.4 g, 16.59 mmol) in anhydrous dioxane (50 mL). The reaction mixture was added to a 150 mL pressure vessel, degassed with Ar for 5 min, and heated at 110 °C for 18 h. The reaction mixture was cooled to room temperature mixed with chloroform (50 mL) and filtered through a bed of Celite. The filterate was evaporated, and the residue was dissolved in MeOH (100 mL). Sodium acetate (1.5 g, 19 mmol) and hydroxylamine hydrochloride (0.95 g, 13.7 mmol) were added to the solution, and the mixture was stirred at room temperature for 10 h. MeOH was evaporated, and the residue was partitioned between NaOH solution (1 N, 100 mL) and DCM (100 mL). The organic layer was washed with water (2 × 50 mL) and brine (1 × 20 mL) and dried. Column chromatography of the residue obtained after evaporation of the solvent (SiO_2/$CHCl_3$:MeOH 9:1) gave **9** as a yellow solid (1.3 g, 81%): mp 135−137 °C. ^{1}H NMR (300 MHz, $CDCl_3$) δ 8.04 (d, J = 5.4 Hz, 1 H), 7.17 (d, J = 3.7 Hz, 1 H), 6.42 (d, J = 3.7 Hz, 1 H), 6.35 (d, J = 5.4 Hz, 1 H), 5.64 (s, 2 H), 4.42 (s, 2 H), 3.59−3.45 (m, 2 H), 0.98−0.85 (m, 2 H), −0.06 (s, 9 H).

2-Iodo-4,5-dimethoxy-*N*-(1-((2-(trimethylsilyl)ethoxy)-methyl)-1*H*-pyrrolo[2,3-*b*]pyridin-4-yl)benzamide (10). 2-Iodo-4,5-dimethoxybenzoyl chloride was prepared by heating a mixture of the acid (0.3 mmol, 1 equiv) and thionyl chloride (7 mL) at reflux for 2 h, followed by the removal of excess thionyl chloride under vacuum. A solution of the acid chloride (0.342 g, 0.3 mmol) in anhydrous DCM (5 mL) was added dropwise to an ice-cold solution of the amine **9** (0.4 g, 0.3 mmol) and TEA (10 equiv) in anhydrous DCM (20 mL). The mixture was heated at reflux for 5 h. After cooling to room temperature, the mixture was washed with saturated $NaHCO_3$ solution (1 × 20 mL), water (2 × 20 mL), and brine (1 × 20 mL) and dried with anhydrous sodium sulfate. The residue obtained after the evaporation of DCM was subjected to silica gel column chromatography using $CHCl_3$−EtOAc (8:2) as eluent to yield the desired amide **10** as a creamy white solid (0.43 g, 58%): mp 165−167 °C. ^{1}H NMR (300 MHz, $CDCl_3$) δ 8.37 (d, J = 5.6 Hz, 1 H), 8.20−8.02 (m, 2 H), 7.36 (d, J = 3.8 Hz, 1 H), 7.32 (s, 1 H), 6.66 (s, 1 H), 5.75 (s, 2 H), 3.95 (s, 3 H), 3.93 (s, 3 H), 3.63−2.57 (m, 2 H), 1.04−0.78 (m, 2 H), −0.05 (s, 9 H). HRESIMS m/z calcd for $C_{22}H_{28}IN_3O_4Si$ $(MH)^+$ 554.0967, found 554.0968.

General Procedures for the Synthesis of Compounds 11a−c. A suspension of sodium hydride (0.72 mmol) in anhydrous DMF (5 mL) was cooled in an ice bath. A solution of **10** (0.2 g, 0.36 mmol) in DMF (2 mL) was added dropwise to the sodium hydride suspension over 5 min. The mixture was stirred at 21 °C for 1 h, and then the appropriate alkyl bromide (0.72 mmol) was added all at once. The reaction mixture was stirred at room temperature for 18 h and then quenched with ice-cold water (25 mL). The mixture was extracted with EtOAc (3 × 15 mL), and the combined organic layers were washed with water (2 × 15 mL) and brine (1 × 20 mL) and dried. Purification of the residue obtained after evaporating the EtOAc layer by silica gel column chromatography ($CHCl_3$−EtOAc, 8:2) yielded **11a−c**.

*tert-Butyl N-(2-Iodo-4,5-dimethoxybenzoyl)-N-(1-((2-(trimethylsilyl)ethoxy)methyl)-1H-pyrrolo[2,3-b]pyridin-4-yl)-glycinate (**11a**).* Compound **11a** was obtained as a creamy white solid (0.22 g, 91%): mp 113−115 °C. ^{1}H NMR (300 MHz, $CDCl_3$) δ 8.17 (s, 1 H), 7.42 (d, J = 3.6 Hz, 1 H), 7.11 (s, 1 H), 7.05−6.99 (m, 1 H), 6.78 (s, 1 H), 6.67 (s, 1 H), 5.76 (s, 2 H), 4.54 (s, 1 H), 3.80 (s, 2 H), 3.61−3.52 (m, 2 H), 3.47 (s, 2 H), 1.50 (s, 9 H), 0.96−0.87 (m,

DOI: 10.1021/acs.jmedchem.8b00510
J. Med. Chem. XXXX, XXX, XXX−XXX

2 H), −0.06 (s, 9 H). HRESIMS *m/z* calcd for $C_{28}H_{38}IN_3O_6Si$ $(MH)^+$ 668.1647, found 668.1644.

*Methyl N-(2-Iodo-4,5-dimethoxybenzoyl)-N-(1-((2-(trimethylsilyl)ethoxy)methyl)-1H-pyrrolo[2,3-b]pyridin-4-yl)-glycinate (**11b**).* This compound was isolated as a yellow oil (0.2 g, 88%). ^{1}H NMR (300 MHz, $CDCl_3$) δ 8.17 (d, J = 5.4 Hz, 1 H), 7.41 (d, J = 3.6 Hz, 1 H), 7.09 (s, 1 H), 7.04 (d, J = 5.4 Hz, 1 H), 6.74 (d, J = 3.6 Hz, 1 H), 6.62 (s, 1 H), 5.70 (s, 2 H), 4.67 (s, 2 H), 3.80 (s, 3 H), 3.78 (s, 3 H), 3.58−3.47 (m, 2 H), 3.44 (s, 3 H), 0.97−0.82 (m, 2 H), −0.08 (s, 9 H). HRESIMS *m/z* calcd for $C_{25}H_{32}IN_3O_4Si$ $(MH)^+$ 626.1177, found 626.1176.

*Ethyl 2-(2-Iodo-4,5-dimethoxy-N-(1-((2-(trimethylsilyl)ethoxy)-methyl)-1H-pyrrolo[2,3-b]pyridin-4-yl)benzamido)butanoate (**11c**).* This compound was isolated as a yellow oil (0.2 g, 83%). ^{1}H NMR (300 MHz, $CDCl_3$) δ 8.16 (d, J = 5.0 Hz, 1 H), 7.38 (d, J = 3.7 Hz, 1 H), 7.10−7.02 (m, 2 H), 6.92 (d, J = 3.7 Hz, 1 H), 6.53 (s, 1 H), 5.66 (s, 2 H), 4.67−4.56 (m, 1 H), 4.32 (d, J = 7.3 Hz, 3 H), 3.75 (s, 3 H), 3.51−3.45 (m, 2 H), 3.36 (s, 3 H), 1.62−1.53 (m, 5 H), 1.36 (t, J = 7.1 Hz, 3 H), 1.01 (t, J = 7.3 Hz, 3 H), 0.93−0.84 (m, 3 H), −0.09 (s, 9 H). HRESIMS *m/z* calcd for $C_{28}H_{38}IN_3O_6Si$ $(MH)^+$ 668.1647, found 668.1651.

***tert*-Butyl 2-(7,8-Dimethoxy-5-oxo-1-((2-(trimethylsilyl)-ethoxy)methyl)-1,5-dihydro-4*H*-benzo[*c*]pyrrolo[2,3-*h*][1,6]-naphthyridin-4-yl)acetate (12a).** $Pd(OAc)_2$ (9 mg, 0.037 mmol), K_2CO_3 (0.15 g, 1.12 mmol), Ag_2CO_3 (0.2 g, 0.74 mmol), and $PCy_3 \cdot HBF_4$ (28 mg, 0.075 mmol) were added to a solution of benzamide **11a** (0.25 g, 0.37 mmol) in DMA (5 mL). The reaction mixture was heated at 130 °C under Ar atmosphere for 18 h. The reaction mixture was cooled to room temperature, and EtOAc (10 mL) was then added. The mixture was filtered through a bed of Celite, and the residue was washed thoroughly with EtOAc (20 mL). The filtrate was transferred to a separatory funnel and washed with water (5 × 15 mL) and brine (15 mL) to remove DMA. The organic layer was dried and evaporated, and the residue was purified by silica gel column chromatography using $CHCl_3$−MeOH (9:1) as the eluent to give the tetracyclic compound **12a** (0.15 g, 74%) as a yellow solid: mp 156−158 °C. ^{1}H NMR (300 MHz, $CDCl_3$) δ 9.18 (s, 1 H), 7.93 (s, 1 H), 7.71 (s, 1 H), 7.40 (d, J = 3.9 Hz, 1 H), 6.81 (d, J = 3.5 Hz, 1 H), 5.79 (s, 2 H), 5.45 (s, 2 H), 4.12 (s, 3 H), 4.04 (s, 3 H), 3.65−3.47 (m, 3 H), 1.53−1.41 (m, 9 H), 1.03−0.78 (m, 2 H), −0.05 (m, 9 H). HRESIMS *m/z* calcd for $C_{28}H_{27}N_3O_6Si$ $(MH)^+$ 540.2524, found 540.2522.

Methyl 2-(7,8-Dimethoxy-5-oxo-1-((2-(trimethylsilyl)-ethoxy)methyl)-1,5-dihydro-4*H*-benzo[*c*]pyrrolo[2,3-*h*][1,6]-naphthyridin-4-yl)acetate (12b). Using the same procedure used for **12a**, compound **12b** was prepared from **11b** and was isolated as a yellow solid (0.1 g, 62%): mp 136−138 °C. ^{1}H NMR (300 MHz, $CDCl_3$) δ 9.18 (s, 1 H), 7.91 (s, 1 H), 7.70 (s, 1 H), 7.40 (d, J = 3.7 Hz, 1 H), 6.76 (d, J = 3.8 Hz, 1 H), 5.81 (s, 2 H), 5.56 (s, 2 H), 4.12 (s, 3 H), 4.04 (s, 3 H), 3.80 (s, 3 H), 3.69−3.54 (m, 2 H), 1.00−0.84 (m, 2 H), −0.04 (s, 9 H). HRESIMS *m/z* calcd for $C_{25}H_{31}N_3O_6Si$ $(MH)^+$ 498.2055, found 498.2047.

Ethyl 2-(7,8-Dimethoxy-5-oxo-1-((2-(trimethylsilyl)ethoxy)-methyl)-1,5-dihydro-4*H*-benzo[*c*]pyrrolo[2,3-*h*][1,6]-naphthyridin-4-yl)butanoate (12c). This compound was prepared from **11c** by the same procedure used for **12a** and isolated as a yellow solid (0.09 g, 44%): mp 152−154 °C. ^{1}H NMR (300 MHz, $CDCl_3$) δ 9.19 (s, 1 H), 7.85 (s, 1 H), 7.70 (s, 1 H), 7.42 (d, J = 3.6 Hz, 1 H), 6.83 (s, 1 H), 5.78 (s, 2 H), 4.11 (s, 3 H), 4.01 (s, 3 H), 3.67−3.54 (m, 3 H), 3.48 (q, J = 7.0 Hz, 3 H), 2.54−2.47 (m, 2 H), 0.94−0.87 (m, 2 H), −0.04 (s, 9 H). HRESIMS *m/z* calcd for $C_{28}H_{37}IN_3O_6Si$ $(MH)^+$ 540.2524, found 540.2523.

***tert*-Butyl 2-(7,8-Dimethoxy-5-oxo-1,5-dihydro-4*H*-benzo-[*c*]pyrrolo[2,3-*h*][1,6]naphthyridin-4-yl)acetate (13a).** Compound **12a** (0.1 g, 0.18 mmol) was dissolved in DCM (5 mL), and TFA (5 mL) was added to the solution dropwise. The mixture was stirred at room temperature for 2 h, and then the solvent was evaporated. The residue obtained was dissolved in MeOH (5 mL) and NaOH solution (2N, 2 mL). Ethylenediamine (1 mL) was added, and the mixture was stirred overnight at room temperature. The mixture was acidified with TFA and extracted with $CHCl_3$ (3 × 10 mL). The combined organic layer was washed with water and brine (15 mL each), dried, and evaporated to yield **13a** as a white solid (20 mg, 26%): mp 212−214 °C. IR (thin film) 2926, 1744, 1647, 1612, 1583, 1462, 1427, 1389, 1244, 1327, 1244, 1225, 1210, 1156, 1107, 1029 cm^{-1}. ^{1}H NMR (300 MHz, DMSO-d_6) δ 12.19−12.08 (s, 1 H), 9.42 (s, 1 H), 8.32 (s, 1 H), 8.12−8.04 (m, 1 H), 7.72 (s, 1 H), 7.58−7.46 (m, 1 H), 6.67−6.58 (m, 1 H), 5.38 (s, 2 H), 4.06 (s, 3 H), 3.91 (s, 3 H), 1.44 (s, 9 H). MALDIMS *m/z* 410 $(MH)^+$. HRESIMS calcd for $C_{22}H_{23}N_3O_5$ $(MH)^+$ 410.1711, found 410.1709. C18 HPLC purity: 96.64% (MeOH−H_2O, 85:15).

Methyl 2-(7,8-Dimethoxy-5-oxo-1,5-dihydro-4*H*-benzo[*c*]-pyrrolo[2,3-*h*][1,6]naphthyridin-4-yl)acetate (13b). This compound was prepared form **12b** using the procedure described for **13a** and was isolated as a white solid (25 mg, 45%): mp 212−214 °C. IR (thin film) 2964, 1752, 1658, 1612, 1575, 1513, 1458, 1427, 1387, 1370, 1351, 1302, 1267, 1242, 1177, 1167, 1143, 1105, 1077, 1003 cm^{-1}. ^{1}H NMR (300 MHz, DMSO-d_6) δ 12.16 (s, 1 H), 9.41 (s, 1 H), 8.06 (s, 1 H), 7.70 (s, 1 H), 7.51 (s, 1 H), 6.59 (s, 1 H), 5.48 (s, 2 H), 4.05 (s, 3 H), 3.90 (d, J = 3.8 Hz, 3 H), 3.71 (d, J = 5.8 Hz, 3 H). MALDIMS *m/z* 368 $(MH)^+$. HRESIMS calcd for $C_{19}H_{17}N_3O_5$ $(MH)^+$ 368.1241, found 368.1243. C18 HPLC purity: 98% (MeOH−H_2O, 85:15).

Ethyl 2-(7,8-Dimethoxy-5-oxo-1,5-dihydro-4*H*-benzo[*c*]-pyrrolo[2,3-*h*][1,6]naphthyridin-4-yl)butanoate (13c). This compound was prepared form compound **12c** using the procedure described for **13a** and was isolated as a white solid (37 mg, 60%): mp 235−237 °C. IR (thin film) 2979, 1725, 1640, 1610, 1572, 1514, 1460, 1420, 1386, 1368, 1339, 1318, 1269, 1244, 1211, 1141, 1110, 1090, 1033, 1014 cm^{-1}. ^{1}H NMR (300 MHz, DMSO-d_6) δ 12.18 (s, 1 H), 9.41 (s, 1 H), 8.04 (s, 1 H), 7.64 (s, 1 H), 7.53 (s, 1 H), 6.95 (s, 1 H), 5.73 (d, J = 7.6 Hz, 1 H), 4.06 (d, J = 4.7 Hz, 1 H), 4.04 (s, 3 H), 3.88 (s, 3 H), 2.37−2.31 (m, 2 H), 1.05 (t, J = 7.1 Hz, 3 H), 0.79 (t, J = 7.5 Hz, 3 H). MALDIMS *m/z* 410 $(MH)^+$. HRESIMS calcd for $C_{22}H_{23}N_3O_5$ $(MH)^+$ 410.1711, found 410.1711. C18 HPLC purity: 100% (MeOH−H_2O, 85:15).

Preparation of the Amides 14a−l. 2-Bromo-3,4-dimethoxybenzoic acid (0.3 g, 1.14 mmol) was added to thionyl chloride (4 mL) and a catalytic amount of DMF. The reaction mixture was heated at reflux for 3 h, and then the thionyl chloride was evaporated to afford the corresponding acid chloride. The appropriate amine (1.2 mmol) was dissolved in DCM (5 mL) in an ice bath and mixed with TEA (5 mmol) in a vial, and the acid chloride was dissolved in DCM (2 mL) and added dropwise to the amine solution. The reaction mixture was stirred overnight at room temperature, and then the reaction was quenched with a saturated solution of sodium carbonate. The organic layer was then separated, washed with water, dried, and evaporated to give a residue. The residue was purified with silica gel column chromatography using either $CHCl_3$−MeOH or EtOAc−hexanes mixtures to give the amides **14a−l** as white solids.

*2-Bromo-N-cyclohexyl-4,5-dimethoxybenzamide (**14a**).* This compound was isolated as a white solid (0.35 g, 89%): mp 185−187 °C. ^{1}H NMR (300 MHz, $CDCl_3$) δ 7.21 (s, 1 H), 6.98 (s, 1 H), 6.17−6.10 (m, 1 H), 3.99 (s, 1 H), 3.89 (s, 6 H), 2.09−1.99 (m, 2 H), 1.80−1.70 (m, 2 H), 1.50−1.17 (m, 6 H). HRESIMS *m/z* calcd for $C_{15}H_{20}BrNO_3$ $(MH)^+$ 342.0699/344.0681, found 342.0701/344.0683.

*2-Bromo-N-(cyclohexylmethyl)-4,5-dimethoxybenzamide (**14b**).* This compound was isolated as a white solid (0.38 g, 93%): mp 163−165 °C. ^{1}H NMR (300 MHz, $CDCl_3$) δ 7.25 (s, 1 H), 6.99 (s, 1 H), 6.33 (s, 1 H), 3.90 (s, 3 H), 3.31 (s, 3 H), 3.31 (t, J = 6.3 Hz, 2 H), 1.89−1.65 (m, 6 H), 1.33−1.12 (m, 4 H), 1.13−0.94 (m, 2 H). HRESIMS *m/z* calcd for $C_{16}H_{22}BrNO_3$ $(MH)^+$ 356.0856/358.0837, found 356.0855/358.0833.

*2-Bromo-N-cycloheptyl-4,5-dimethoxybenzamide (**14c**).* This compound was isolated as a white solid (0.36 g, 88%): mp 157−158 °C. ^{1}H NMR (300 MHz, $CDCl_3$) δ 7.20 (s, 1 H), 6.98 (s, 1 H), 6.20 (d, J = 7.8 Hz, 1 H), 4.23−4.12 (m, 1 H), 3.89 (s, 6 H), 2.12−2.01 (m, 2 H), 1.76−1.50 (m, 13 H). HRESIMS *m/z* calcd for $C_{16}H_{22}BrNO_3$ $(MH)^+$ 356.0856/358.0837, found 356.0855/358.0837.

DOI: 10.1021/acs.jmedchem.8b00510
J. Med. Chem. XXXX, XXX, XXX−XXX

*2-Bromo-N-cyclooctyl-4,5-dimethoxybenzamide (**14d**).* This compound was isolated as a white solid (0.32 g, 75%): mp 145−147 °C. ^{1}H NMR (300 MHz, $CDCl_3$) δ 7.21 (s, 1 H), 6.99 (s, 1 H), 6.23 (d, J = 8.0 Hz, 1 H), 4.27−4.14 (m, 1 H), 3.89 (s, 6 H), 2.03−1.90 (m, 2 H), 1.75−1.50 (m, 15 H). HRESIMS m/z calcd for $C_{17}H_{24}BrNO_3$ $(MH)^+$ 370.1012/372.0994, found 370.1012/372.0997.

*2-Bromo-4,5-dimethoxy-N-(1-methylpiperidin-4-yl)benzamide (**14e**).* This compound was isolated as a white solid (0.35 g, 85%): mp 201−204 °C. ^{1}H NMR (300 MHz, $CDCl_3$) δ 7.19 (s, 1 H), 6.99 (s, 1 H), 6.17 (s, 1 H), 4.06−3.96 (m, 1 H), 3.89 (s, 6 H), 2.90−2.79 (m, 2 H), 2.33 (s, 3 H), 2.27−2.18 (m, 2 H), 2.14−2.04 (m, 2 H), 1.74−1.60 (m, 2 H). HRESIMS m/z calcd for $C_{15}H_{21}BrN_2O_3$ $(MH)^+$ 357.0808/359.0789, found 357.0809/359.0791.

*tert-Butyl 4-(2-Bromo-4,5-dimethoxybenzamido)piperidine-1-carboxylate (**14f**).* This compound was isolated as a white solid (0.4 g, 79%): mp 210−215 °C. ^{1}H NMR (300 MHz, $CDCl_3$) δ 7.19 (s, 1 H), 6.97 (s, 1 H), 6.20 (d, J = 7.9 Hz, 1 H), 4.18−3.98 (m, 3 H), 3.89 (s, 6 H), 3.03−2.91 (m, 2 H), 2.06−1.97 (m, 2 H), 1.46 (s, 9 H). HRESIMS m/z calcd for $C_{19}H_{27}BrN_2O_3$ $(MNa)^+$ 465.0995/467.0977, found 465.0995/467.0977.

*tert-Butyl (R)-3-(2-Bromo-4,5-dimethoxybenzamido)pyrrolidine-1-carboxylate (**14g**).* This compound was isolated as a white solid (0.38 g, 77%): mp 241−243 °C. ^{1}H NMR (300 MHz, $CDCl_3$) δ 7.23 (s, 1 H), 6.99 (s, 1 H), 6.39 (s, 1 H), 4.68−4.61 (m, 1 H), 3.90 (s, 6 H), 3.68 (dd, J = 11.5, 5.9 Hz, 1 H), 3.53−3.45 (m, 2 H), 3.41−3.37 (m, 1 H), 2.28−2.17 (m, 1 H), 2.08−1.95 (m, 1 H), 1.47 (s, 9 H). HRESIMS m/z calcd for $C_{18}H_{25}BrN_2O_5$ $(MNa)^+$ 451.0839/453.0821, found 451.0836/453.0819.

*tert-Butyl (R)-3-(2-Bromo-4,5-dimethoxybenzamido)piperidine-1-carboxylate (**14h**).* This compound was isolated as a white solid (0.41 g, 80%): mp 235−236 °C. ^{1}H NMR (300 MHz, $CDCl_3$) δ 7.27 (s, 1 H), 6.99 (s, 1 H), 6.51 (d, J = 7.3 Hz, 1 H), 4.24−4.15 (s, 1 H), 3.90 (s, 6 H), 3.63−3.51 (m, 3 H), 3.35−3.20 (m, 1 H), 1.93−1.71 (m, 3 H), 1.44 (s, 9 H). HRESIMS m/z calcd for $C_{19}H_{27}BrN_2O_5$ $(MNa)^+$ 465.0995/467.0977, found 465.0991/467.0979.

*Methyl (2-Bromo-4,5-dimethoxybenzoyl)-D-valinate (**14i**).* This compound was isolated as a white solid (0.38 g, 88%): mp 178−180 °C. ^{1}H NMR (300 MHz, $CDCl_3$) δ 7.02 (s, 1 H), 6.86 (d, J = 8.4 Hz, 1 H), 4.78 (dd, J = 8.6, 4.7 Hz, 1 H), 3.91 (s, 3 H), 3.89 (s, 3 H), 3.78 (s, 3 H), 2.37−2.28 (m, 1 H), 1.06 (d, J = 6.9 Hz, 3 H), 1.02 (d, J = 6.9 Hz, 3 H). HRESIMS m/z calcd for $C_{15}H_{20}BrNO_5$ $(MNa)^+$ 396.0417/398.0398, found 396.0412/398.0392.

*Methyl (2-Bromo-4,5-dimethoxybenzoyl)-L-valinate (**14j**).* This compound was isolated as a white solid (0.37 g, 87%): mp 181−183 °C. ^{1}H NMR (300 MHz, $CDCl_3$) δ 7.02 (s, 1 H), 6.86 (d, J = 8.6 Hz, 1 H), 4.78 (dd, J = 8.6, 4.7 Hz, 1 H), 3.91 (s, 3 H), 3.89 (s, 3 H), 3.78 (s, 3 H), 2.38−2.24 (m, 1 H), 1.06 (d, J = 6.9 Hz, 3 H), 1.02 (d, J = 6.9 Hz, 3 H). HRESIMS m/z calcd for $C_{15}H_{20}BrNO_5$ $(MNa)^+$ 396.0417/398.0398, found 396.0421/398.0403.

*Methyl (R)-2-(2-Bromo-4,5-dimethoxybenzamido)butanoate (**14k**).* This compound was isolated as a white solid (0.34 g, 82%): mp 165−168 °C. ^{1}H NMR (300 MHz, $CDCl_3$) δ 7.26 (s, 1 H), 7.02 (s, 1 H), 6.91 (d, J = 7.8 Hz, 1 H), 4.79 (dd, J = 13.0, 6.5 Hz, 1 H), 3.91 (s, 3 H), 3.89 (s, 3 H), 3.80 (s, 3 H), 2.13−1.97 (m, 1 H), 1.92−1.85 (m, 1 H), 1.02 (t, J = 7.5 Hz, 3 H). HRESIMS m/z calcd for $C_{14}H_{18}BrNO_5$ $(MNa)^+$ 382.0260/384.0241, found 382.0258/384.0237.

*Methyl (S)-2-(2-Bromo-4,5-dimethoxybenzamido)butanoate (**14l**).* This compound was isolated as a white solid (0.37 g, 89%): mp 185−187 °C. ^{1}H NMR (300 MHz, $CDCl_3$) δ 7.25 (s, 1 H), 7.01 (s, 1 H), 6.92 (d, J = 7.1 Hz, 1 H), 4.82−4.75 (m, 1 H), 3.91 (s, 3 H), 3.89 (s, 3 H), 3.79 (s, 3 H), 2.12−1.97 (m, 1 H), 1.91−1.85 (m, 1 H), 1.01 (t, J = 7.5 Hz, 3 H). HRESIMS m/z calcd for $C_{14}H_{18}BrNO_5$ $(MNa)^+$ 382.0260/384.0241, found 382.0263/384.0246.

General Procedure for the Synthesis of Compounds 16a−l. A screw-capped vial with a Teflon cap was charged with SEM-protected 4-iodo-7-azaindole (**15**) (0.26 mmol, 1 equiv), amides **14a−l** (0.26 mmol, 1.05 equiv), $Pd(OTFA)_2$ (10 mol %), TFP (20 mol %), norborene (0.26 mmol, 1.05 equiv), and cesium carbonate (3 equiv). The atmosphere of the vial was evacuated and refilled with argon once and then the solvent (4 mL) was added via syringe and the vial was evacuated and refilled with argon twice. The reaction mixture was heated at the stated temperatures and time in Table 2 and was then cooled to room temperature. The reaction mixture was filtered through a pad of Celite and the solvent was evaporated and the residue obtained was loaded on a silica gel column and the mixture was purified using EtOAc-hexane mixture to give compounds **16a−l**.

*4-Cyclohexyl-7,8-dimethoxy-1-((2-(trimethylsilyl)ethoxy)methyl)-1,4-dihydro-5H-benzo[c]pyrrolo[2,3-h][1,6]naphthyridin-5-one (**16a**).* Compound **16a** was isolated as a yellowish powder (0.1 g, 78%): mp 198−200 °C. ^{1}H NMR (500 MHz, $CDCl_3$) δ 9.18 (s, 1 H), 7.93 (s, 1 H), 7.71−7.67 (m, 1 H), 7.45 (d, J = 3.7 Hz, 1 H), 6.83 (d, J = 3.8 Hz, 1 H), 5.82 (s, 2 H), 5.02−4.95 (m, 1 H), 4.16 (s, 3 H), 4.09 (s, 3 H), 3.72−3.59 (m, 2 H), 3.08−2.91 (m, 2 H), 2.12−2.01 (m, 4 H), 1.86 (s, 1 H), 1.57−1.49 (m, 3 H), 1.05−0.95 (m, 2 H), 0.02 (s, 9 H). HRESIMS m/z calcd for $C_{28}H_{37}N_3O_4Si$ $(MH)^+$ 508.2626, found 508.2629.

*4-(Cyclohexylmethyl)-7,8-dimethoxy-1-((2-(trimethylsilyl)ethoxy)methyl)-1,4-dihydro-5H-benzo[c]pyrrolo[2,3-h][1,6]naphthyridin-5-one (**16b**).* This compound was isolated as a yellow solid (0.11 g, 81%): mp 122−123 °C. ^{1}H NMR (300 MHz, $CDCl_3$) δ 9.18 (s, 1 H), 7.93 (s, 1 H), 7.70 (s, 1 H), 7.42 (d, J = 3.7 Hz, 1 H), 6.85 (d, J = 3.8 Hz, 1 H), 5.80 (s, 2 H), 4.11 (s, 3 H), 4.05 (s, 3 H), 3.68−3.52 (m, 2 H), 1.73−1.61 (m, 9 H), 1.27−1.18 (m, 3 H), 1.01−0.85 (m, 2 H), −0.04 (s, 9 H). HRESIMS m/z calcd for $C_{29}H_{39}N_3O_4Si$ $(MH)^+$ 522.2782, found 522.2780.

*4-Cycloheptyl-7,8-dimethoxy-1-((2-(trimethylsilyl)ethoxy)methyl)-1,4-dihydro-5H-benzo[c]pyrrolo[2,3-h][1,6]naphthyridin-5-one (**16c**).* This compound was isolated as a yellowish-white solid (70 mg, 50%): mp 184−186 °C. ^{1}H NMR (500 MHz, $CDCl_3$) δ 9.20 (s, 1 H), 7.94 (s, 1 H), 7.73 (s, 1 H), 7.46 (d, J = 3.7 Hz, 1 H), 6.94 (d, J = 3.7 Hz, 1 H), 5.81 (d, J = 8.7 Hz, 2 H), 5.24 (d, J = 10.4 Hz, 1 H), 4.16 (s, 3 H), 4.09 (s, 3 H), 3.71−3.55 (m, 3 H), 2.99−2.85 (m, 2 H), 2.18−2.08 (m, 2 H), 2.01 (s, 2 H), 1.80 (d, J = 4.3 Hz, 4 H), 1.71−1.63 (m, 7 H), 1.06−0.96 (m, 3 H), 0.02 (s, 9 H). HRESIMS m/z calcd for $C_{29}H_{39}N_3O_4Si$ $(MH)^+$ 522.2782, found 522.2782.

*4-Cyclooctyl-7,8-dimethoxy-1-((2-(trimethylsilyl)ethoxy)methyl)-1,4-dihydro-5H-benzo[c]pyrrolo[2,3-h][1,6]naphthyridin-5-one (**16d**).* This compound was isolated as a creamy white powder (84 mg, 58%): mp 166−168 °C. ^{1}H NMR (500 MHz, $CDCl_3$) δ 9.20 (s, 1 H), 7.93 (s, 1 H), 7.72 (d, J = 10.5 Hz, 1 H), 7.47 (d, J = 3.7 Hz, 1 H), 6.96 (d, J = 3.8 Hz, 1 H), 5.81 (d, J = 9.8 Hz, 2 H), 5.28−5.22 (m, 1 H), 4.16 (s, 3 H), 4.09 (s, 3 H), 3.71−3.59 (m, 2 H), 3.00−2.89 (m, 2 H), 2.13−2.07 (m, 2 H), 2.05−1.96 (m, 3 H), 1.89−1.78 (m, 2 H), 1.74−1.63 (m, 7 H), 1.05−0.98 (m, 2 H), 0.02 (s, 9 H). HRESIMS m/z calcd for $C_{30}H_{41}N_3O_4Si$ $(MH)^+$ 536.2939, found 536.2939.

*7,8-Dimethoxy-4-(1-methylpiperidin-4-yl)-1-((2-(trimethylsilyl)ethoxy)methyl)-1,4-dihydro-5H-benzo[c]pyrrolo[2,3-h][1,6]naphthyridin-5-one (**16e**).* This compound was isolated as a yellow oil (85 mg, 60%). ^{1}H NMR (500 MHz, $CDCl_3$) δ 9.18 (s, 1 H), 7.92 (s, 1 H), 7.72 (s, 1 H), 7.47 (d, J = 3.5 Hz, 1 H), 6.80 (s, 1 H), 5.82 (s, 2 H), 5.02 (s, 1 H), 4.16 (s, 3 H), 4.10 (s, 3 H), 3.69−3.61 (m, 2 H), 3.46−3.39 (m, 2 H), 3.24 (s, 2 H), 2.53 (s, 2 H), 2.02−1.96 (m, 2 H), 1.06−0.94 (m, 2 H), 0.02 (s, 9 H). HRESIMS m/z calcd for $C_{28}H_{38}N_4O_4Si$ $(MH)^+$ 523.2735, found 523.2737.

*tert-Butyl 4-(7,8-Dimethoxy-5-oxo-1-((2-(trimethylsilyl)ethoxy)methyl)-1,5-dihydro-4H-benzo[c]pyrrolo[2,3-h][1,6]naphthyridin-4-yl)piperidine-1-carboxylate (**16f**).* This compound was isolated as a yellowish white solid (95 mg, 58%): mp 189−192 °C. ^{1}H NMR (500 MHz, $CDCl_3$) δ 9.19 (s, 1 H), 7.90 (s, 1 H), 7.72 (s, 1 H), 7.48 (d, J = 3.7 Hz, 1 H), 6.78 (d, J = 3.7 Hz, 1 H), 5.84 (s, 2 H), 5.15−5.11 (m, 1 H), 4.51−4.42 (m, 2 H), 4.16 (s, 3 H), 4.10 (s, 3 H), 3.71−3.62 (m, 2 H), 3.26−3.16 (m, 2 H), 2.98 (s, 2 H), 1.95 (s, 2 H), 1.57 (s, 9 H), 1.05−0.95 (m, 2 H), 0.02 (s, 9 H). HRESIMS m/z calcd for $C_{32}H_{44}N_4O_6Si$ $(MH)^+$ 609.3102, found 609.3102.

*tert-Butyl (R)-3-(7,8-Dimethoxy-5-oxo-1-((2-(trimethylsilyl)ethoxy)methyl)-1,5-dihydro-4H-benzo[c]pyrrolo[2,3-h][1,6]naphthyridin-4-yl)pyrrolidine-1-carboxylate (**16g**).* This compound

DOI: 10.1021/acs.jmedchem.8b00510
J. Med. Chem. XXXX, XXX, XXX−XXX

was isolated as a creamy white solid (95 mg, 60%): mp 156−158 °C. ^{1}H NMR (500 MHz, $CDCl_3$) δ 9.20 (s, 1 H), 7.91 (s, 1 H), 7.73 (s, 1 H), 7.50 (s, 1 H), 6.88 (s, 1 H), 5.84 (s, 2 H), 4.17 (s, 3 H), 4.10 (s, 3 H), 4.04−4.01 (m, 1 H), 3.93−3.89 (m, 1 H), 3.73−3.69 (m, 1 H), 3.67−3.62 (m, 2 H), 3.09−3.02 (m, 1 H), 2.46−2.42 (m, 1 H), 1.56 (s, 9 H), 1.05−0.96 (m, 2 H), 0.02 (s, 9 H). HRESIMS m/z calcd for $C_{31}H_{42}N_4O_6Si$ $(MH)^+$ 595.2946, found 595.2949.

*tert-Butyl (R)-3-(7,8-Dimethoxy-5-oxo-1-((2-(trimethylsilyl)-ethoxy)methyl)-1,5-dihydro-4H-benzo[c]pyrrolo[2,3-h][1,6]-naphthyridin-4-yl)piperidine-1-carboxylate (**16h**).* This compound was isolated as a yellowish solid (82 mg, 52%): mp 148−152 °C. ^{1}H NMR (300 MHz, $CDCl_3$) δ 9.13 (s, 1 H), 7.82 (s, 1 H), 7.64 (s, 1 H), 7.40 (d, J = 3.7 Hz, 1 H), 7.00−6.92 (m, 1 H), 5.81 (s, 2 H), 4.98−4.92 (m, 1 H), 4.53−4.41 (m, 1 H), 4.28−4.22 (m, 1 H), 4.11 (s, 3 H), 4.03 (s, 3 H), 3.66−3.56 (m, 2 H), 3.08−3.03 (m, 1 H), 2.92−2.79 (m, 2 H), 2.07−2.02 (m, 1 H), 1.89 (s, 2 H), 1.65 (s, 9 H), 1.26 (t, J = 7.2 Hz, 2 H), 0.99−0.89 (m, 1 H), −0.04 (s, 9 H). HRESIMS m/z calcd for $C_{32}H_{44}N_4O_6Si$ $(MH)^+$ 609.3102, found 609.3104.

*Methyl (R)-2-(7,8-Dimethoxy-5-oxo-1-((2-(trimethylsilyl)ethoxy)-methyl)-1,5-dihydro-4H-benzo[c]pyrrolo[2,3-h][1,6]naphthyridin-4-yl)-3-methylbutanoate (**16i**).* This compound was isolated as a yellow powder (0.1 g, 76%): mp 212−214 °C. ^{1}H NMR (500 MHz, $CDCl_3$) δ 9.27 (s, 1 H), 7.91 (s, 1 H), 7.78 (s, 1 H), 7.49 (d, J = 3.8 Hz, 1 H), 6.95 (d, J = 3.8 Hz, 1 H), 5.83 (t, J = 7.1 Hz, 2 H), 5.51 (d, J = 9.3 Hz, 1 H), 4.18 (s, 3 H), 4.09 (s, 3 H), 3.76 (s, 3 H), 3.71−3.62 (m, 2 H), 3.29−3.22 (m, 1 H), 1.49 (d, J = 6.6 Hz, 3 H), 1.35−1.26 (m, 1 H), 1.04−0.93 (m, 2 H), 0.78 (d, J = 7.1 Hz, 3 H), 0.02 (s, 9 H). HRESIMS m/z calcd for $C_{28}H_{37}N_3O_6Si$ $(MH)^+$ 540.2524, found 540.2524.

*Methyl (S)-2-(7,8-Dimethoxy-5-oxo-1-((2-(trimethylsilyl)ethoxy)-methyl)-1,5-dihydro-4H-benzo[c]pyrrolo[2,3-h][1,6]naphthyridin-4-yl)-3-methylbutanoate (**16j**).* This compound was isolated as a yellowish solid (91 mg, 63%): mp 208−210 °C. ^{1}H NMR (500 MHz, $CDCl_3$) δ 9.27 (s, 1 H), 7.92 (s, 1 H), 7.78 (s, 1 H), 7.48 (d, J = 3.7 Hz, 1 H), 6.94 (d, J = 3.8 Hz, 1 H), 5.82 (t, J = 6.7 Hz, 2 H), 5.51 (d, J = 9.3 Hz, 1 H), 4.17 (s, 3 H), 4.08 (s, 3 H), 3.76 (d, J = 6.7 Hz, 3 H), 3.72−3.64 (m, 2 H), 3.29−3.21 (m, 1 H), 2.17 (s, 1 H), 1.49 (d, J = 6.6 Hz, 3 H), 1.03−0.95 (m, 2 H), 0.78 (d, J = 7.1 Hz, 3 H), 0.02 (s, 9 H). HRESIMS m/z calcd for $C_{28}H_{37}N_3O_6Si$ $(MH)^+$ 540.2524, found 540.2524.

*Methyl (R)-2-(7,8-Dimethoxy-5-oxo-1-((2-(trimethylsilyl)ethoxy)-methyl)-1,5-dihydro-4H-benzo[c]pyrrolo[2,3-h][1,6]naphthyridin-4-yl)butanoate (**16k**).* This compound was isolated as a yellowish powder (0.1 g, 68%): mp 189−193 °C. ^{1}H NMR (500 MHz, $CDCl_3$) δ 9.19 (s, 1 H), 7.85 (s, 1 H), 7.71 (s, 1 H), 7.42 (d, J = 3.6 Hz, 1 H), 6.81 (d, J = 3.6 Hz, 1 H), 5.80−5.72 (m, 2 H), 5.65 (t, J = 7.2 Hz, 1 H), 4.13 (s, 3 H), 4.04 (s, 3 H), 3.74 (s, 3 H), 3.62−3.55 (m, 2 H), 2.66−2.58 (m, 1 H), 2.42−2.37 (m, 1 H), 1.00 (t, J = 7.5 Hz, 3 H), 0.95−0.89 (m, 2 H), −0.05 (s, 9 H). HRESIMS m/z calcd for $C_{27}H_{35}N_3O_6Si$ $(MH)^+$ 526.2368, found 526.2370.

*Methyl (S)-2-(7,8-Dimethoxy-5-oxo-1-((2-(trimethylsilyl)ethoxy)-methyl)-1,5-dihydro-4H-benzo[c]pyrrolo[2,3-h][1,6]naphthyridin-4-yl)butanoate (**16l**).* This compound was isolated as a yellowish solid (0.072 g, 55%): mp 188−192 °C. ^{1}H NMR (500 MHz, $CDCl_3$) δ 9.19 (s, 1 H), 7.85 (s, 1 H), 7.71 (s, 1 H), 7.42 (d, J = 3.6 Hz, 1 H), 6.81 (d, J = 3.6 Hz, 1 H), 5.80−5.72 (m, 2 H), 5.65 (t, J = 7.2 Hz, 1 H), 4.13−4.08 (m, 4 H), 4.10−3.98 (m, 3 H), 3.74 (s, 3 H), 3.62−3.55 (m, 2 H), 2.65−2.59 (m, 1 H), 2.43−2.37 (m, 1 H), 1.00 (t, J = 7.5 Hz, 3 H), 0.95−0.89 (m, 2 H), −0.05 (s, 9 H). HRESIMS m/z calcd for $C_{27}H_{35}N_3O_6Si$ $(MH)^+$ 526.2368, found 526.2370.

General Procedure for the Deprotection of Compounds 17a−j. Compounds **16a−j** (0.1 mmol) were dissolved in DCM (2 mL), and TFA (2 mL) was added to the solution dropwise. The mixture was stirred at room temperature for 2 h, and then the solvent was evaporated. The residue was dissolved in MeOH (5 mL), and ethylenediamine (1 mL) was added and the mixture was stirred overnight at 50 °C. The mixture was acidified with TFA and extracted with $CHCl_3$ (3 × 10 mL). The combined organic layer was washed with water and brine (15 mL each), dried, and evaporated to yield **17a−j** as white solids.

*4-Cyclohexyl-7,8-dimethoxy-1,4-dihydro-5H-benzo[c]pyrrolo-[2,3-h][1,6]naphthyridin-5-one (**17a**).* This compound was isolated as a white solid (28 mg, 74%): mp 233−235 °C. IR (thin film) 3120, 3002, 2922, 2847, 1654, 1608, 1576, 1509, 1462, 1450, 1417, 1400, 1378, 1357, 1300, 1224, 1207, 1180, 1124, 1040 cm^{-1}. ^{1}H NMR (500 MHz, DMSO-d_6) δ 12.08 (s, 1 H), 9.30 (s, 1 H), 7.95 (s, 1 H), 7.64 (s, 1 H), 7.54−7.45 (m, 1 H), 6.58 (s, 1 H), 4.85 (s, 1 H), 3.99 (s, 3 H), 3.85 (s, 3 H), 2.85−2.71 (m, 2 H), 1.89−1.81 (m, 4 H), 1.75−1.67 (m, 1 H), 1.48−1.38 (m, 2 H), 1.27−1.19 (m, 2 H). MALDIMS m/z 378 $(MH)^+$. HRESIMS calcd for $C_{22}H_{23}N_3O_3$ $(MH)^+$ 378.1812, found 378.1814. C18 HPLC purity: 100% (MeOH−H_2O, 85:15).

*4-(Cyclohexylmethyl)-7,8-dimethoxy-1,4-dihydro-5H-benzo[c]-pyrrolo[2,3-h][1,6]naphthyridin-5-one (**17b**).* This compound was isolated as a white solid (32 mg, 82%): mp 198−199 °C. IR (thin film) 3314, 2922, 2849, 1654, 1634, 1573, 1511, 1463, 1450, 1422, 1385, 1358, 1325, 1259, 1206, 1178, 1124, 1051, 1009 cm^{-1}. ^{1}H NMR (300 MHz, DMSO-d_6) δ 12.09 (s, 1 H), 9.38 (s, 1 H), 8.31 (s, 1 H), 8.02 (s, 1 H), 7.72 (s, 1 H), 7.54 (s, 1 H), 6.76 (s, 1 H), 4.61 (s, 2 H), 4.03 (s, 3 H), 3.89 (s, 3 H), 1.84−1.78 (m, 1 H), 1.68−1.59 (m, 5 H), 1.25−0.94 (m, 6 H). MALDIMS m/z 392 $(MH)^+$. HRESIMS calcd for $C_{23}H_{25}N_3O_3$ $(MH)^+$ 392.1969, found 392.1968. C18 HPLC purity: 97.15% (MeOH−H_2O, 85:15).

*4-Cycloheptyl-7,8-dimethoxy-1,4-dihydro-5H-benzo[c]pyrrolo-[2,3-h][1,6]naphthyridin-5-one (**17c**).* This compound was isolated as a white solid (35 mg, 89%): mp 242−244 °C. IR (thin film) 3120, 2926, 2849, 1651, 1610, 1576, 1508, 1462, 1449, 1397, 1356, 1310, 1258, 1240, 1208, 1175, 1120, 1069 cm^{-1}. ^{1}H NMR (500 MHz, DMSO-d_6) δ 12.15 (s, 1 H), 9.38 (s, 1 H), 8.02 (s, 1 H), 7.71 (s, 1 H), 7.57 (dd, J = 10.7, 7.4 Hz, 1 H), 6.75 (s, 1 H), 5.17 (s, 1 H), 4.05 (s, 3 H), 3.92 (s, 3 H), 2.85−2.63 (m, 2 H), 2.04−1.92 (m, 4 H), 1.71−1.54 (m, 6 H), 1.25 (s, 3 H). ^{13}C NMR (126 MHz, DMSO) δ 161.75, 153.94, 149.54, 149.27, 141.05, 138.16, 128.85, 124.90, 118.46, 108.07, 107.86, 106.16, 103.20, 100.94, 61.68, 56.51, 55.79, 32.49, 28.21, 26.20. MALDIMS m/z 392 $(MH)^+$. HRESIMS calcd for $C_{23}H_{25}N_3O_3$ $(MH)^+$ 392.1969, found 392.1969. C18 HPLC purity: 96.89% (MeOH−H_2O, 85:15).

*4-Cyclooctyl-7,8-dimethoxy-1,4-dihydro-5H-benzo[c]pyrrolo-[2,3-h][1,6]naphthyridin-5-one (**17d**).* This compound was isolated as a white solid (32 mg, 79%): mp 235−238 °C. IR (thin film) 2918, 1644, 1607, 1571, 1510, 1463, 1416, 1378, 1354, 1334, 1263, 1241, 1207, 1180, 1164, 1062 cm^{-1}. ^{1}H NMR (500 MHz, DMSO-d_6) δ 12.16 (s, 1 H), 9.38 (s, 1 H), 8.02 (s, 1 H), 7.71 (s, 1 H), 7.60 (s, 1 H), 6.75 (s, 1 H), 5.18 (s, 1 H), 4.05 (s, 3 H), 3.92 (s, 3 H), 2.82−2.75 (m, 2 H), 1.98−1.83 (m, 4 H), 1.81−1.71 (m, 2 H), 1.64−1.50 (m, 5 H), 1.29−1.21 (m, 2 H). MALDIMS m/z 406 $(MH)^+$. HRESIMS calcd for $C_{24}H_{27}N_3O_3$ $(MH)^+$ 406.2125, found 406.2127. C18 HPLC purity: 96.27% (MeOH−H_2O, 85:15).

*7,8-Dimethoxy-4-(1-methylpiperidin-4-yl)-1,4-dihydro-5H-benzo[c]pyrrolo[2,3-h][1,6]naphthyridin-5-one (**17e**).* This compound was isolated as a white solid (25 mg, 63%): mp 215−217 °C. IR (thin film) 2936, 1633, 1607, 1569, 1512, 1463, 1418, 1353, 1334, 1309, 1258, 1231, 1185, 1143, 1125, 1037, 1011 cm^{-1}. ^{1}H NMR (500 MHz, DMSO-d_6) δ 12.14 (s, 1 H), 9.33 (s, 1 H), 7.97 (s, 1 H), 7.64 (s, 1 H), 7.53 (d, J = 3.4 Hz, 1 H), 6.65 (s, 1 H), 5.04−4.98 (m, 1 H), 4.00 (s, 3 H), 3.86 (s, 3 H), 2.98−2.82 (m, 8 H), 2.57−2.54 (m, 1 H), 2.02−1.80 (m, 2 H). MALDIMS m/z 393 $(MH)^+$. HRESIMS calcd for $C_{22}H_{24}N_4O_3$ $(MH)^+$ 393.1921, found 393.1926. C18 HPLC purity: 99.09% (MeOH−H_2O, 85:15).

*7,8-Dimethoxy-4-(piperidin-4-yl)-1,4-dihydro-5H-benzo[c]-pyrrolo[2,3-h][1,6]naphthyridin-5-one (**17f**).* This compound was isolated as a white solid (18 mg, 48%): mp 258−259 °C. IR (thin film) 2925, 1635, 1610, 1572, 1515, 1313, 1261, 1210, 1038 cm^{-1}. ^{1}H NMR (500 MHz, DMSO-d_6) δ 12.07 (s, 1 H), 9.31 (s, 1 H), 7.95 (s, 1 H), 7.64 (s, 1 H), 7.51 (s, 1 H), 6.61 (s, 1 H), 4.98−4.89 (m, 1 H), 3.99 (s, 3 H), 3.86 (s, 3 H), 3.21−3.08 (m, 3 H), 2.89 (d, J = 8.6 Hz, 2 H), 2.69−2.58 (m, 4 H), 1.79−1.69 (m, 2 H). MALDIMS m/z 379 $(MH)^+$. HRESIMS calcd for $C_{21}H_{22}N_4O_3$ $(MH)^+$ 379.1764, found 379.1762. C18 HPLC purity: 99.27% (MeOH−H_2O, 85:15).

*(R)-7,8-Dimethoxy-4-(pyrrolidin-3-yl)-1,4-dihydro-5H-benzo[c]-pyrrolo[2,3-h][1,6]naphthyridin-5-one (**17g**).* This compound was

DOI: 10.1021/acs.jmedchem.8b00510
J. Med. Chem. XXXX, XXX, XXX−XXX

isolated as a white solid (10 mg, 27%): mp 274−276 °C. IR (thin film) 2920, 1939, 1608, 1570, 1511, 1455, 1419, 1398, 1379, 1336, 1310, 1262, 1244, 1208, 1161, 1127, 1026 cm^{-1}. ^1H NMR (500 MHz, DMSO-d_6) δ 12.16 (s, 1 H), 9.39 (s, 1 H), 8.04 (s, 1 H), 7.72 (s, 1 H), 7.58 (s, 1 H), 6.96 (s, 1 H), 5.72 (s, 1 H), 4.06 (s, 3 H), 3.92 (s, 3 H), 3.31−3.21 (m, 2 H), 3.05−2.91 (m, 1 H), 2.38−2.28 (m, 2 H), 0.95−0.84 (m, 1 H). MALDIMS m/z 365 $(MH)^+$. HRESIMS calcd for $C_{20}H_{20}N_4O_3$ $(MH)^+$ 365.1608, found 365.1610. C18 HPLC purity: 100% (MeOH−H_2O, 85:15).

*(R)-7,8-Dimethoxy-4-(piperidin-3-yl)-1,4-dihydro-5H-benzo[c]-pyrrolo[2,3-h][1,6]naphthyridin-5-one (**17h**).* This compound was isolated as a white solid (18 mg, 48%): mp 286−287 °C. IR (thin film) 3130, 2919, 1649, 1610, 1577, 1509, 1463, 1407, 1378, 1334, 1310, 1242, 1209, 1175, 1127, 1022 cm^{-1}. ^1H NMR (500 MHz, DMSO-d_6) δ 12.13 (s, 1 H), 9.37 (s, 1 H), 8.02 (s, 1 H), 7.69 (s, 1 H), 7.57 (s, 1 H), 6.86 (s, 1 H), 5.03−4.97 (m, 1 H), 4.06 (s, 3 H), 3.92 (s, 3 H), 3.88−2.84 (m, 1 H), 3.14−3.08 (m, 1 H), 3.02−2.96 (m, 2 H), 1.93−1.85 (m, 1 H), 1.84−1.78 (m, 1 H), 1.68−1.60 (m, 1 H). MALDIMS m/z 379 $(MH)^+$. HRESIMS calcd for $C_{21}H_{22}N_4O_3$ $(MH)^+$ 379.1764, found 379.1765. C18 HPLC purity: 99.29% (MeOH−H_2O, 85:15).

*Methyl (R)-2-(7,8-Dimethoxy-5-oxo-1,5-dihydro-4H-benzo[c]-pyrrolo[2,3-h][1,6]naphthyridin-4-yl)-3-methylbutanoate (**17i**).* This compound was isolated as a white solid (12 mg, 29%): mp 256−258 °C. IR (thin film) 2922, 1726, 1608, 1572, 1514, 1461, 1420, 1386, 1334, 1268, 1184, 1137, 1021 cm^{-1}. ^1H NMR (500 MHz, DMSO-d_6) δ 12.29 (s, 1 H), 9.47 (s, 1 H), 8.09 (s, 1 H), 7.69 (s, 1 H), 7.64−7.53 (m, 1 H), 6.91 (s, 1 H), 5.54 (d, J = 9.3 Hz, 1 H), 4.08 (s, 3 H), 3.93 (s, 3 H), 3.57 (s, 3 H), 3.10−2.90 (m, 1 H), 1.37 (d, J = 6.6 Hz, 3 H), 0.61 (d, J = 7.1 Hz, 3 H). MALDIMS m/z 410 $(MH)^+$. HRESIMS calcd for $C_{22}H_{23}N_3O_5$ $(MH)^+$ 410.1711, found 410.1712. C18 HPLC purity: 100% (MeOH−H_2O, 85:15).

*Methyl (S)-2-(7,8-Dimethoxy-5-oxo-1,5-dihydro-4H-benzo[c]-pyrrolo[2,3-h][1,6]naphthyridin-4-yl)-3-methylbutanoate (**17j**).* This compound was isolated as a white solid (26 mg, 68%): mp 274−276 °C. IR (thin film) 2956, 1741, 1652, 1608, 1570, 1513, 1461, 1420, 1384, 1365, 1334, 1314, 1264, 1246, 1210, 1145, 1119, 1071, 1028 cm^{-1}. ^1H NMR (500 MHz, DMSO-d_6) δ 12.21 (s, 1 H), 9.40 (s, 1 H), 8.03 (s, 1 H), 7.63 (s, 1 H), 7.57−7.47 (m, 1 H), 6.85 (s, 1 H), 5.48 (d, J = 9.2 Hz, 1 H), 4.02 (s, 3 H), 3.87 (s, 3 H), 3.51 (s, 3 H), 3.01−2.91 (m, 1 H), 1.31 (d, J = 6.6 Hz, 3 H), 0.55 (d, J = 7.1 Hz, 3 H). MALDIMS m/z 410 $(MH)^+$. HRESIMS calcd for $C_{22}H_{23}N_3O_5$ $(MH)^+$ 410.1711, found 410.1710. C18 HPLC purity: 98.30% (MeOH−H_2O, 85:15).

(R)-2-(7,8-Dimethoxy-5-oxo-1,5-dihydro-4*H*-benzo[*c*]-pyrrolo[2,3-*h*][1,6]naphthyridin-4-yl)butanoic Acid (17k). Compound **16k** (0.14 g, 0.226 mmol) was dissolved in DCM (2 mL), and TFA (2 mL) was added to the solution dropwise. The mixture was stirred at room temperature for 2 h, and then the solvent was evaporated. The residue was dissolved in MeOH (5 mL) and THF (5 mL) and ethylenediamine (1 mL) and NaOH (2 mL, 1 M aq solution) were added and the mixture was stirred overnight at 60 °C. The volatile solvents were removed, and the solution was acidified with HCl to pH 3. The mixture was extracted with EtOAc (3 × 10 mL). The combined organic layer was washed with water and brine (15 mL each), dried, and evaporated to yield **17k** as a white solid (80 mg, 81%): mp 212−214 °C. IR (thin film) 3262, 2921, 1722, 1657, 1608, 1574, 1463, 1422, 1387, 1338, 1314, 1264, 1246, 1211, 1137, 1082 cm^{-1}. ^1H NMR (500 MHz, DMSO-d_6) δ 12.15 (s, 1 H), 9.38 (s, 1 H), 8.02 (s, 1 H), 7.63 (s, 1 H), 7.50 (s, 1 H), 6.90 (s, 1 H), 5.64 (s, 1 H), 4.02 (s, 3 H), 3.86 (s, 3 H), 2.30−2.23 (m, 2 H), 0.78 (t, J = 7.5 Hz, 3 H). MALDIMS m/z 382 $(MH)^+$. HRESIMS calcd for $C_{20}H_{19}N_3O_5$ $(MH)^+$ 382.1397, found 382.1397.

(S)-2-(7,8-Dimethoxy-5-oxo-1,5-dihydro-4*H*-benzo[*c*]-pyrrolo[2,3-*h*][1,6]naphthyridin-4-yl)butanoic Acid (17l). Following the same procedure used for **17k**, compound **17l** was isolated as a white solid (84 mg, 85%): mp 217−218 °C. IR (thin film) 3544, 2937, 1704, 1676, 1601, 1515, 1459, 1425, 1390, 1330, 1310, 1264, 1229, 1211, 1181, 1147, 1028 cm^{-1}. ^1H NMR (500 MHz, DMSO-d_6) δ 12.24 (s, 1 H), 9.45 (s, 1 H), 8.08 (s, 1 H), 7.69 (s, 1 H), 7.58 (s, 1 H), 6.98 (s, 1 H), 5.70 (s, 1 H), 4.08 (s, 3 H), 3.93 (s, 3 H), 2.48−2.37 (m, 2 H), 2.32 (d, J = 6.6 Hz, 1 H), 0.85 (t, J = 7.5 Hz, 3 H). MALDIMS m/z 382 $(MH)^+$. HRESIMS calcd for $C_{20}H_{19}N_3O_5$ $(MH)^+$ 382.1397, found 382.1399.

(R)-2-(7,8-Dimethoxy-5-oxo-1,5-dihydro-4*H*-benzo[*c*]-pyrrolo[2,3-*h*][1,6]naphthyridin-4-yl)-3-methylbutanoic Acid (17m). Compound **16i** (0.1 mmol) was dissolved in DCM (2 mL), and TFA (2 mL) was added to the solution dropwise. The mixture was stirred at room temperature for 2 h, and then the solvent was evaporated. The residue was dissolved in MeOH (5 mL) and THF (5 mL) and ethylenediamine (1 mL) and NaOH (2 mL, 1 M soln) were added and the mixture was stirred overnight at 60 °C. The volatile solvents were removed, and the solution was acidified with HCl to pH 3. The mixture was extracted with EtOAc (3 × 10 mL). The combined organic layer was washed with water and brine (15 mL each), dried, and evaporated to yield **17m** as a yellow solid (0.11 g, 96%): mp 198−200 °C. IR (thin film) 3513, 2968, 1720, 1665, 1606, 1514, 1459, 1442, 1388, 1329, 1264, 1183, 1136, 1017 cm^{-1}. ^1H NMR (500 MHz, DMSO-d_6) δ 12.22 (s, 1 H), 9.40 (s, 1 H), 8.02 (s, 1 H), 7.68 (m, 1 H), 7.60−7.40 (m, 1 H), 6.82 (s, 1 H), 5.35 (d, J = 9.3 Hz, 1 H), 4.02 (s, 3 H), 3.87 (s, 3 H), 3.12−2.94 (m, 1 H), 1.32 (d, J = 8.6 Hz, 3 H), 0.56 (d, J = 7.1 Hz, 3 H). MALDIMS m/z 396 $(MH)^+$. HRESIMS calcd for $C_{21}H_{21}N_3O_5$ $(MH)^+$ 396.1554, found 396.1553.

(R)-3-(3-(7,8-Dimethoxy-5-oxo-1,5-dihydro-4*H*-benzo[*c*]-pyrrolo[2,3-*h*][1,6]naphthyridin-4-yl)piperidin-1-yl)-3-oxopropanenitrile (18). Compound **17h** (30 mg, 0.08 mol) was added to a solution of HATU (30 mg, 0.08 mmol), DIPEA (30 mg 0.24 mmol), and cyanoacetic acid (5 mg) in DMF (4 mL). The mixture was stirred at room temperature for 24 h and then quenched with saturated ammonium chloride (15 mL). The solution was extracted with EtOAc (3 × 15 mL). The combined organic layer was washed with saturated sodium bicarbonate (15 mL), water, and brine and dried using anhydrous sodium sulfate. The residue obtained after evaporation of the organic layer was purified using column chromatography (CH_2Cl_2−MeOH 9.8:0.2) to give compound **18** as white solid (26 mg, 73%): mp 185−187 °C. IR (thin film) 2928, 2262, 1645, 1608, 1573, 1512, 1446, 1417, 1378, 1333, 1308, 1261, 1208, 1129, 1063 cm^{-1}. ^1H NMR (500 MHz, DMSO-d_6) δ 12.11 (s, 1 H), 9.33 (s, 1 H), 7.98 (s, 1 H), 7.64 (d, J = 4.1 Hz, 1 H), 7.51 (d, J = 12.7 Hz, 1 H), 6.59 (m, 1 H), 4.82 (s, 1 H), 4.68−4.61 (m, 1 H), 4.48−4.42 (m, 1 H), 4.24−4.18 (m, 1 H), 4.13−4.08 (m, 1 H), 3.99 (s, 3 H), 3.86 (s, 3 H), 3.76−3.70 (m, 2 H), 3.11−3.02 (m, 1 H), 2.93−2.84 (m, 2 H), 2.50 (s, 2 H), 1.88−1.84 (m, 1 H), 1.72−1.65 (m, 1 H). MALDIMS m/z 446 $(MH)^+$. HRESIMS calcd for $C_{24}H_{23}N_5O_4$ $(MH)^+$ 446.1823, found 446.1822. C18 HPLC purity: 95.85% (MeOH−H_2O, 85:15).

(R)-1-(2-(7,8-Dimethoxy-5-oxo-1,5-dihydro-4*H*-benzo[*c*]-pyrrolo[2,3-*h*][1,6]naphthyridin-4-yl)-3-methylbutanoyl)-azetidine-3-carbonitrile (19a). Following the same procedure used for compound **18** and starting with **17m**, compound **19a** was isolated as a white solid (48 mg, 86%): mp 236−238 °C. IR (thin film) 3248, 2965, 1649, 1608, 1570, 1514, 1413, 1367, 1332, 1264, 1210, 1138, 1115, 1022 cm^{-1}. ^1H NMR (500 MHz, DMSO-d_6) δ 12.25 (s, 1 H), 9.42 (s, 1 H), 8.03 (s, 1 H), 7.66 (s, 1 H), 7.58 (s, 1 H), 7.05−6.88 (m, 1 H), 5.48 (s, 1 H), 4.02 (s, 3 H), 4.00−3.95 (m, 1 H), 3.88 (s, 3 H), 3.83−3.79 (m, 1 H), 3.45−3.41 (m, 1 H), 3.07−3.01 (m, 1 H), 1.26 (d, J = 6.6 Hz, 3 H), 0.50 (d, J = 7.2 Hz, 3 H). ^{13}C NMR (126 MHz, DMSO-d_6) δ 160.95, 154.52, 149.78, 149.44, 141.44, 138.14, 129.34, 126.42, 124.97, 116.50, 108.29, 107.52, 105.77, 103.52, 101.91, 56.63, 55.84, 26.69, 21.76, 18.10. MALDIMS m/z 460 $(MH)^+$. HRESIMS calcd for $C_{25}H_{25}N_5O_4$ $(MH)^+$ 460.1979, found 460.1981. C18 HPLC purity: 100% (MeOH−H_2O, 85:15).

(R)-2-(7,8-Dimethoxy-5-oxo-1,5-dihydro-4*H*-benzo[*c*]-pyrrolo[2,3-*h*][1,6]naphthyridin-4-yl)-3-methyl-*N*-(2,2,2-trifluoroethyl)butanamide (19b). Following the same procedure used for compound **18** and starting with **17m**, compound **19b** was isolated as a white solid (45 mg, 74%): mp 247−248 °C. IR (thin film) 3123, 2970, 2878, 1677, 1627, 1608, 1548, 1514, 1465, 1418, 1397, 1387, 1362, 1334, 1309, 1282, 1233, 1213, 1159, 1120, 1063, 1034 cm^{-1}. ^1H NMR (500 MHz, DMSO-d_6) δ 12.17 (s, 1 H), 9.40 (s, 1 H), 8.63 (t, J = 6.3 Hz, 1 H), 8.03 (s, 1 H), 7.64 (s, 1 H), 7.53 (s, 1

DOI: 10.1021/acs.jmedchem.8b00510
J. Med. Chem. XXXX, XXX, XXX−XXX

H), 6.82 (s, 1 H), 5.25 (d, J = 9.5 Hz, 1 H), 4.02 (s, 3 H), 3.99−3.95 (m, 1 H), 3.86 (s, 3 H), 3.73−3.68 (m, 1 H), 3.04−2.96 (m, 1 H), 1.19 (d, J = 6.5 Hz, 3 H), 0.38 (d, J = 6.8 Hz, 3 H). MALDIMS m/z 477 $(MH)^+$. HRESIMS calcd for $C_{23}H_{23}F_3N_4O_4$ $(MH)^+$ 477.1744, found 477.1744. C18 HPLC purity: 97.59% (MeOH−H_2O, 85:15).

(*R*)-1-(2-(7,8-Dimethoxy-5-oxo-1,5-dihydro-4*H*-benzo[*c*]-pyrrolo[2,3-*h*][1,6]naphthyridin-4-yl)butanoyl)azetidine-3-carbonitrile (20a). Compound **17k** (30 mg, 0.08 mmol) was added to a solution of HATU (30 mg, 0.08 mmol) and DIPEA (30 mg 0.24 mmol) in DMF (4 mL). After stirring for 5 min, azetidine-3-carbonitrile hydrochloride (13 mg, 0.09 mmol) was added to the mixture. The mixture was stirred at room temperature for 24 h, and then the reaction was quenched with saturated ammonium chloride (15 mL). The solution was extracted with EtOAc (3 × 15 mL). The combined organic layer was washed with saturated sodium bicarbonate (15 mL), water, and brine and dried using anhydrous sodium sulfate. The residue obtained after evaporation of the organic layer was purified using silica gel column chromatography (CH_2Cl_2:MeOH 9.8:0.2) to yield compound **20a** as a white solid (28 mg, 60%): mp 257−260 °C. IR (thin film) 3313, 2957, 1649, 1609, 1572, 1514, 1464, 1421, 1385, 1310, 1262, 1209, 1152, 1040 cm^{-1}. ^1H NMR (500 MHz, DMSO-d_6) δ 12.26 (s, 1 H), 9.47 (s, 1 H), 8.09 (s, 1 H), 7.72 (s, 1 H), 7.62 (s, 1 H), 7.06 (s, 1 H), 5.77 (s, 1 H), 4.08 (s, 3 H), 4.03−3.97 (m, 1 H), 3.94 (s, 3 H), 3.91−3.86 (m, 1 H), 3.54 (s, 1 H), 2.47−2.36 (m, 2 H), 2.21 (d, J = 7.6 Hz, 1 H), 0.81 (t, J = 7.6 Hz, 3 H). MALDIMS m/z 446 $(MH)^+$. HRESIMS calcd for $C_{24}H_{23}N_5O_4$ $(MH)^+$ 446.1823, found 446.1828. C18 HPLC purity: 96.72% (MeOH−H_2O, 85:15).

(*R*)-2-(7,8-Dimethoxy-5-oxo-1,5-dihydro-4*H*-benzo[*c*]-pyrrolo[2,3-*h*][1,6]naphthyridin-4-yl)-*N*-(2,2,2-trifluoroethyl)-butanamide (20b). Compound **17k** (30 mg, 0.08 mmol) was added to a solution of HATU (30 mg, 0.08 mmol) and DIPEA (30 mg 0.24 mmol) in DMF (4 mL). After stirring for 5 min, trifluoroethylamine hydrochloride (11 mg, 0.09 mmol) was added to the mixture. The mixture was stirred at room temperature for 24 h and then quenched with saturated ammonium chloride (15 mL). The solution was extracted with EtOAc (3 × 15 mL). The combined organic layer was washed with saturated sodium bicarbonate (15 mL), water, and brine and dried using anhydrous sodium sulfate. The residue obtained after evaporation of the organic layer was purified using silica gel column chromatography (CH_2Cl_2:MeOH 9.8:0.2) to provide compound **20b** as a white solid (20 mg, 55%): mp 267−268 °C. IR (thin film) 3508, 2979, 2872, 2249, 1649, 1610, 1572, 1517, 1499, 1416, 1386, 1315, 1247, 1210, 1186, 1166, 1112, 1041 cm^{-1}. ^1H NMR (500 MHz, DMSO-d_6) δ 12.10 (s, 1 H), 9.37 (s, 1 H), 8.50 (t, J = 6.4 Hz, 1 H), 8.02 (s, 1 H), 7.62 (s, 1 H), 7.49 (s, 1 H), 6.64 (s, 1 H), 5.56 (t, J = 7.5 Hz, 1 H), 4.01 (s, 3 H), 3.86 (s, 3 H), 3.68−3.61 (m, 2 H), 2.65 (s, 1 H), 2.37−2.29 (m, 2 H), 0.52 (t, J = 7.4 Hz, 3 H). MALDIMS m/z (rel intensity) 463 $(MH)^+$. HRESIMS calcd for $C_{22}H_{21}F_3N_4O_4$ $(MH)^+$ 463.1588, found 463.1602. C18 HPLC purity: 98.86% (MeOH−H_2O, 85:15).

(*S*)-2-(7,8-Dimethoxy-5-oxo-1,5-dihydro-4*H*-benzo[*c*]-pyrrolo[2,3-*h*][1,6]naphthyridin-4-yl)-*N*-(2,2,2-trifluoroethyl)-butanamide (21). Following the same procedure used for **20b** but using the acid **17l**, compound **21** was isolated as a white solid (24 mg, 60%): mp 235−237 °C. IR (thin film) 3318, 2959, 1699, 1649, 1610, 1572, 1513, 1465, 1421, 1365, 1337, 1310, 1260, 1248, 1208, 1151, 1136 cm^{-1}. ^1H NMR (500 MHz, DMSO-d_6) δ 12.16 (s, 1 H), 9.43 (s, 1 H), 8.56 (t, J = 6.3 Hz, 1 H), 8.08 (s, 1 H), 7.68 (s, 1 H), 7.58−7.52 (m, 1 H), 6.70 (s, 1 H), 5.62 (t, J = 7.6 Hz, 1 H), 4.08 (s, 3 H), 4.07−3.99 (m, 1 H), 3.92 (s, 3 H), 3.71 (s, 2 H), 2.39 (t, J = 7.5 Hz, 3 H), 0.59 (t, J = 7.4 Hz, 3 H). MALDIMS m/z 463 $(MH)^+$. HRESIMS calcd for $C_{22}H_{21}F_3N_4O_4$ $(MH)^+$ 463.1588, found 463.1590. C18 HPLC purity: 100% (MeOH−H_2O, 85:15).

Enzyme Inhibition Assay. The enzyme assay was performed by Reaction Biology Corporation according to the following protocol: The base reaction buffer consisted of 20 mM Hepes (pH 7.5), 10 mM $MgCl_2$, 1 mM EDTA, 0.02% Brij-35, 0.02 mg/mL BSA, 0.1 mM Na_3VO_4, 2 mM DTT, and 1% DMSO. The indicated substrate was added to freshly prepared base reaction buffer, and then the required cofactors were added to the substrate solution. Purified JAK kinases were added into the substrate solution and gently mixed. A solution of the compounds in DMSO was then added into the kinase reaction mixture by Acoustic technology (Echo550; nanoliter range), and the mixture was incubated for 20 min at room temperature. ^{33}P-ATP (specific activity 10 Ci/mmol) was then added into the reaction mixture to initiate the reaction. The kinase reaction was incubated for 2 h at room temperature, and then the mixtures were spotted onto P81 ion exchange paper. Finally, the kinase activity was detected by the filter-binding method.

STAT-5 Phosphorylation Inhibition Assay. The experiments performed by Reaction Biology Corporation. SZ4 cells from growing stock were seeded in 96-well plates at 1 × 10^5 cells/well in 100 μL of complete media and then incubated overnight at 37 °C, 5% CO_2. The cells were treated with test compounds (starting at 30 μM, 8 doses with 3-fold dilution) for 1 h. The cells were then stimulated with hIL-2 at a final concentration of 100 ng/mL for 15 min. The cells were spun down, and the culture medium was aspirated. The cells were lysed with 50 μL of 1× cell lysis buffer. The cell lysates (25 μL) were used for MSD assay immediately or stored at −80 °C. MSD assay was performed according to the kit manual (https://www.mesoscale.com/~/media/files/product%20inserts/phospho%20tyr694%20total%20stat5a%20b%20wcl.pdf). IC_{50} values were calculated using GraphPad Prism 4 based on a sigmoidal dose−response equation. Western blot assay experimental details are provided in the Supporting Information.

Primary T Cell Inhibition Assay. $CD4^+$ T cells were isolated from mouse spleen and cultured in vitro with antibodies to CD3 (5 μg/mL) and CD28 (2 μg/mL) in the presence of IL-2 (100 U/mL) for nonpolarizing conditions as described before.[41] Inhibitors were added to culture at the indicated concentrations. After culture, the cells were stained with XTT (sodium 2,3,-bis(2-methoxy-4-nitro-5-sulfophenyl)-5-[(phenylamino)-carbonyl]-2*H*-tetrazolium inner salt) and analyzed at 475 nm by a microplate reader (SpectraMax i3X, Molecular Devices). The cells were cultured for 5 days and stained with antibodies to mouse CD4 (RM4-5). The cells were activated with phorbol myristate acetate (PMA, 50 ng/mL, Sigma-Aldrich), ionomycin (1 μM, Sigma-Aldrich), and monensin (2 mM, Sigma-Aldrich) for 4 h followed by fixation with 4% PFA in PBS and permeabilization in 1% saponins in PBS. The cells were stained with antibodies to mouse IFNγ (XGM1.2) or mouse IL-17 (TC11-18H10.1) for flow cytometry (Canto II, Becton Dickinson). For IL-17 production, the T cells were cultured with anti-IL2, anti-IFNγ, anti-IL-4, IL-23, TNF-α, and IL-1β as previously described.[41]

Kinome Scanning Assay. Selected compounds were tested for kinome selectivity at Eurofins DiscoverX Corporation, Fremont, California, USA, by applying their KINOMEscan technology. Different kinases were labeled with a unique DNA tag for qPCR. A known kinase ligand was immobilized on a solid support and incubated with the labeled kinase in the presence of either DMSO or a specified concentration of the test compounds. After equilibration, the solid support was washed to remove unbound kinase, and then the kinase captured on solid support was quantified by qPCR. Finally, the captured kinase levels in the test compound and DMSO control samples were compared.

Pharmacokinetic Profiling. The experiments were performed at Eurofins Scientific Inc., Lancaster, PA, USA.

Caco-2 Permeability. Caco-2 cells were grown in tissue culture flasks, trypsinized, and suspended in medium, and known concentrations of cell suspensions were seeded onto wells of a Millipore 96-well Caco-2 plate. The cells were allowed to grow and differentiate for 3 weeks, feeding at two-day intervals. For apical to basolateral (A → B) permeability, the test article was added to the apical (A) side and the amount of permeation on the basolateral (B) side was determined; for basolateral to apical (B → A) permeability, the test article was added to the B side and the amount of permeation on the A side was determined. To test tight junctions and monolayer integrity, the A-side buffer contained 100 μM Lucifer yellow dye in transport buffer (1.98 g/L glucose in 10 mM HEPES, 1× Hank's Balanced Salt Solution) with pH 6.5, while the B-side buffer was

DOI: 10.1021/acs.jmedchem.8b00510
J. Med. Chem. XXXX, XXX, XXX−XXX

transport buffer with pH 7.4. Caco-2 cells were incubated with these buffers for 2 h, and the receiver-side buffer was removed for analysis by LC/MS/MS. To verify the tight junctions and integrity of Caco-2 cell monolayers, aliquots of the cell buffers were analyzed by fluorescence (Lucifer yellow transport ≤2%). Any deviations from control values are reported. Data are expressed as permeability (P_{app}) = $(dQ/dt)/(C_0A)$ where dQ/dt is the rate of permeation, C_0 is the initial concentration of test agent, and A is the area of the monolayer. In bidirectional permeability studies, the efflux ratio (R_e) is also calculated: $R_e = (P_{app}\ B \rightarrow A)/(P_{app}\ A \rightarrow B)$; $R^e > 2$ indicates a potential substrate for P-glycoprotein or other active efflux transporter(s).

Metabolic Stability Analysis. The compounds were incubated in duplicate with pooled human liver microsomes at 37 °C. The reaction mixtures contained microsomal protein in 100 mM potassium phosphate buffer (pH 7.4), 2 mM NADPH, and 3 mM $MgCl_2$. A control was run for each test article omitting NADPH to detect NADPH-free degradation. At predetermined time points, an aliquot was removed from each experimental and control reaction and mixed with an equal volume of ice-cold methanol containing propranolol as the internal standard to stop the reaction and precipitate proteins. Stopped reactions were kept on ice for at least 10 min followed by an addition of an equal volume of water. The samples were centrifuged to remove precipitated protein, and the supernatants were analyzed by LC-MS/MS to quantify parent remaining. Data was calculated as % parent remaining by assuming zero-minute time point peak area ratio (analyte/IS) as 100% and dividing remaining time point peak area ratios by the zero minute time point peak area ratio. Data were subjected to fit a first-order decay model to calculate slope and thereby half-life.

PBS Solubility Screen. Serial dilutions of the tested compounds, reserpine, tamoxifen, and verapamil were prepared in phosphate buffered saline (PBS) at 100× the final concentration. The solutions were diluted 100-fold into PBS in a 96-well plate and mixed. The absorbance of the PBS-containing plate was measured prior to addition of the test agents to determine the background absorbance. After 2 h, the presence of precipitate was detected by turbidity (absorbance at 540 nm). An absorbance value of greater than (mean + 3× standard deviation of the blank), after subtracting the preexperiment background, is indicative of turbidity. The solubility limit is reported as the highest experimental concentration with no evidence of turbidity.

Molecular Modeling. The X-ray crystal structures of JAK kinases were obtained from the Protein Data Bank (JAK1 PDB 4I5C; JAK2 PDB 3LXK). Each protein structure was cleaned, inspected for errors and missing residues, hydrogens were added, and the water molecules were deleted using Accelry's Discovery studio 2.5 software. Structures of the inhibitors were constructed using ChemBioDraw Ultra 13 and saved in SDF file format and were corrected and optimized using Accelrys Discovery studio 2.5 software. GOLD 4.1 was used for docking with the default parameters except that the iterations were increased to 300000 and the early termination option was disabled. The centroids of the binding sites were defined by the ligands in the cocrystal structures. The top 10 docking poses per ligand were inspected visually following the docking runs. Energy minimizations were performed for selected ligand poses. The CHARMM force field was utilized within the Accelrys Discovery Studio 2.5 for energy minimization.

Collagen-Induced Inflammation Model. All procedures performed on live mice were approved by the Purdue Animal Use and Care Committee and conformed with NIH guidelines. Eight-week-old, male DBA-1 mice were obtained from Jackson Laboratories. The mice were kept in housing facilities that maintained a constant temperature of 22 °C and a constant humidity of 50%. The mice were maintained on a 12-h light/dark cycle. Collagen-induced arthritis was induced in the mice after a one-week acclimation period in our housing facility. To induce the inflammation, equal volumes of the following compounds were mixed on ice with a homogenizer until a stable emulsion formed: 2 mg/mL of bovine type II collagen in 0.05 M acetic acid (Chondrix) and Complete Freund's Adjuvant (Chondrix) containing 4 mg/mL of *Mycoplasma tuberculosis*. Mice were maintained under anesthesia during the inculcation via inhalation of isoflurane. Each mouse received a 100 μL injection of the emulsion transdermally in the tail. Three weeks later, the mice received a booster inculcation the same way but with an emulsion made from equal parts of Incomplete Freund's Adjuvant (Chondrix) and type II bovine collagen (Chondrix). After 8 weeks, all mice displayed symptoms of inflammation. They were sorted into one of the three treatment groups so that the mean RA score for each of the treatment groups was the same, and seven mice were assigned to each treatment group. Sorting in this manner controlled for the variability in the response to a CIA induction. The treatment groups consisted of **17b**, tofacitinib, and vehicle (10% DMSO and 10% Cremophor EL). Daily doses of 5 mg/kg/day were administered subcutaneously in 10% DMSO and 10% Cremophor EL for 5 weeks. Every week inflammation was assessed by measuring paw volume with a digital caliper and scoring all four paws with the 0−4 rheumatoid arthritis score. The paws were scored by a trained technician who was blinded to the treatment groups and who referred to a visual key for scoring every time (Figure 7s, Supporting Information). Paw volume was calculated as the product of the length, width, and height of the paws. Measurements of height and width were taken at the same location on the paw every time. Mouse weight was monitored throughout the treatment period to watch for any toxicities, and no large fluctuations in weight were seen as a result of any of the treatments (Figure 8s, Supporting Information). After 5 weeks of treatment, the mice were euthanized, and the paws were collected for micro CT analysis. The Student's t test revealed that both tofacitinib and **17b** cause a significantly different response compared to the vehicle control and that there is not a statistically significant difference between the two drugs. Statistical significance was determined using the Holm−Sidak method, with $\alpha = 0.05$.

■ ASSOCIATED CONTENT

Supporting Information

The Supporting Information is available free of charge on the ACS Publications website at DOI: 10.1021/acs.jmedchem.8b00510.

Table for the % growth of the NCI-60 cell lines, gels monitoring Top1-mediated DNA cleavage, table of kinome selectivity data, kinome maps, EC_{50} determination curves and experimental procedure for the JAK3-mediated STAT-5 phosphorylation assay, mouse paw collagen-induced inflammation assay (RA paw volume and percent weight change results) (PDF)

SMILES molecular formula strings (CSV)

Figure 9 JAK1 molecular model (PDB)

Figure 9 JAK3 molecular model (PDB)

Figure 10 JAK1 molecular model (PDB)

Figure 10 JAK3 molecular model (PDB)

Figure 11 JAK1 molecular model (PDB)

Figure 11 JAK3 molecular model (PDB)

■ AUTHOR INFORMATION

Corresponding Author

*Phone: (765)494-1465. Fax: (765)494-6970. E-mail: cushman@purdue.edu.

ORCID

Mohamed S. A. Elsayed: 0000-0002-1353-7259

Philip S. Low: 0000-0001-9042-5528

Mark Cushman: 0000-0002-0152-5891

Notes

The authors declare no competing financial interest.

DOI: 10.1021/acs.jmedchem.8b00510
J. Med. Chem. XXXX, XXX, XXX−XXX

■ ACKNOWLEDGMENTS

We gratefully acknowledge support from the Purdue University Center for Cancer Research, and NIH grants P30 CA023168, NIH 5R01AI080769, and NIH R01AI121302. Mohamed S. A. Elsayed was partially supported by the McKeehan Graduate Scholarship in Pharmacy Award. This investigation was also supported by the NCI Center for Cancer Research (Z01 BC006161).

■ ABBREVIATIONS USED

DCM, dichloromethane; DMA, *N*,*N*-dimethylacetamide; DMF, *N*,*N*-dimethylformamide; DMSO, dimethyl sulfoxide; EtOAc, ethyl acetate; HATU, (1-[bis(dimethylamino)-methylene]-1*H*-1,2,3-triazolo[4,5-*b*]pyridinium 3-oxid hexafluorophosphate); MOM, methoxymethyl; SEM, 2-(trimethylsilyl)ethoxymethyl; TEA, triethylamine; TFA, trifluoroacetic acid; THF, tetrahydrofuran

■ REFERENCES

(1) Chaplin, D. D. Overview of the Immune Response. *J. Allergy Clin. Immunol.* **2010**, *125*, S3−23.
(2) Cho, J. H.; Feldman, M. Heterogeneity of Autoimmune Diseases: Pathophysiologic Insights from Genetics and Implications for New Therapies. *Nat. Med.* **2015**, *21*, 730−738.
(3) Cooper, G. S.; Bynum, M. L. K.; Somers, E. C. Recent Insights in the Epidemiology of Autoimmune Diseases: Improved Prevalence Estimates and Understanding of Clustering of Diseases. *J. Autoimmun.* **2009**, *33*, 197−207.
(4) Dembic, Z. Cytokines of the Immune System: Interleukins. In *The Cytokines of the Immune System*; Academic Press: Amsterdam, 2015; Chapter 6, pp 143−239.
(5) Rawlings, J. S.; Rosler, K. M.; Harrison, D. A. The JAK/STAT Signaling Pathway. *J. Cell Sci.* **2004**, *117*, 1281−1283.
(6) Yamaoka, K.; Saharinen, P.; Pesu, M.; Holt, V. E. T.; Silvennoinen, O.; O'Shea, J. J. The Janus Kinases (JAKs). *Genome Biol.* **2004**, *5*, 253.
(7) Clark, J. D.; Flanagan, M. E.; Telliez, J.-B. Discovery and Development of Janus Kinase (JAK) Inhibitors for Inflammatory Diseases. *J. Med. Chem.* **2014**, *57*, 5023−5038.
(8) Furumoto, Y.; Gadina, M. The Arrival of JAK Inhibitors: Advancing the Treatment of Immune and Hematologic Disorders. *BioDrugs* **2013**, *27*, 431−438.
(9) Yamaoka, K. Janus Kinase Inhibitors for Rheumatoid Arthritis. *Curr. Opin. Chem. Biol.* **2016**, *32*, 29−33.
(10) Boyce, E. G.; Vyas, D.; Rogan, E. L.; Valle-Oseguera, C. S.; O'Dell, K. M. Impact of Tofacitinib on Patient Outcomes in Rheumatoid Arthritis − Review of Clinical Studies. *Patient Related Outcome Measures* **2016**, *7*, 1−12.
(11) Biajoli, A. F. P.; Schwalm, C. S.; Limberger, J.; Claudino, T. S.; Monteiro, A. L. Recent Progress in the Use of Pd-Catalyzed C-C Cross-Coupling Reactions in the Synthesis of Pharmaceutical Compounds. *J. Braz. Chem. Soc.* **2014**, *25*, 2186−2214.
(12) Lessing, T.; Müller, T. Sequentially Palladium-Catalyzed Processes in One-Pot Syntheses of Heterocycles. *Appl. Sci.* **2015**, *5*, 1803.
(13) Harris, C. J.; Hill, R. D.; Sheppard, D. W.; Slater, M. J.; Stouten, P. F. W. The Design and Application of Target-Focused Compound Libraries. *Comb. Chem. High Throughput Screening* **2011**, *14*, 521−531.
(14) Garrett, M. D.; Collins, I. Anticancer Therapy with Checkpoint Inhibitors: What, Where and When? *Trends Pharmacol. Sci.* **2011**, *32*, 308−316.
(15) Tse, A. N.; Rendahl, K. G.; Sheikh, T.; Cheema, H.; Aardalen, K.; Embry, M.; Ma, S.; Moler, E. J.; Ni, Z. J.; Lopes de Menezes, D. E.; Hibner, B.; Gesner, T. G.; Schwartz, G. K. Chir-124, a Novel Potent Inhibitor of Chk1, Potentiates the Cytotoxicity of Topoisomerase I Poisons in Vitro and in Vivo. *Clin. Cancer Res.* **2007**, *13*, 591−602.
(16) Bartek, J.; Lukas, J. Chk1 and Chk2 Kinases in Checkpoint Control and Cancer. *Cancer Cell* **2003**, *3*, 421−429.
(17) Matthews, T. P.; Jones, A. M.; Collins, I. Structure-Based Design, Discovery and Development of Checkpoint Kinase Inhibitors as Potential Anti-Cancer Therapies. *Expert Opin. Drug Discovery* **2013**, *8*, 621−640.
(18) Aris, S. M.; Pommier, Y. Potentiation of the Novel Topoisomerase I Inhibitor Indenoisoquinoline LMP-400 by the Cell Checkpoint and Chk1-Chk2 Inhibitor Azd7762. *Cancer Res.* **2012**, *72*, 979−989.
(19) Brnardic, E. J.; Garbaccio, R. M.; Fraley, M. E.; Tasber, E. S.; Steen, J. T.; Arrington, K. L.; Dudkin, V. Y.; Hartman, G. D.; Stirdivant, S. M.; Drakas, B. A.; Rickert, K.; Walsh, E. S.; Hamilton, K.; Buser, C. A.; Hardwick, J.; Tao, W.; Beck, S. C.; Mao, X.; Lobell, R. B.; Sepp-Lorenzino, L.; Yan, Y.; Ikuta, M.; Munshi, S. K.; Kuo, L. C.; Kreatsoulas, C. Optimization of a Pyrazoloquinolinone Class of Chk1 Kinase Inhibitors. *Bioorg. Med. Chem. Lett.* **2007**, *17*, 5989−5994.
(20) Gaulton, A.; Bellis, L. J.; Bento, A. P.; Chambers, J.; Davies, M.; Hersey, A.; Light, Y.; McGlinchey, S.; Michalovich, D.; Al-Lazikani, B.; Overington, J. P. Chembl: A Large-Scale Bioactivity Database for Drug Discovery. *Nucleic Acids Res.* **2012**, *40*, D1100−D1107.
(21) Kulagowski, J. J.; Blair, W.; Bull, R. J.; Chang, C.; Deshmukh, G.; Dyke, H. J.; Eigenbrot, C.; Ghilardi, N.; Gibbons, P.; Harrison, T. K.; Hewitt, P. R.; Liimatta, M.; Hurley, C. A.; Johnson, A.; Johnson, T.; Kenny, J. R.; Bir Kohli, P.; Maxey, R. J.; Mendonca, R.; Mortara, K.; Murray, J.; Narukulla, R.; Shia, S.; Steffek, M.; Ubhayakar, S.; Ultsch, M.; van Abbema, A.; Ward, S. I.; Waszkowycz, B.; Zak, M. Identification of Imidazo-Pyrrolopyridines as Novel and Potent JAK1 Inhibitors. *J. Med. Chem.* **2012**, *55*, 5901−5921.
(22) Van Epps, S.; Fiamengo, B.; Edmunds, J.; Ericsson, A.; Frank, K.; Friedman, M.; George, D.; George, J.; Goedken, E.; Kotecki, B.; Martinez, G.; Merta, P.; Morytko, M.; Shekhar, S.; Skinner, B.; Stewart, K.; Voss, J.; Wallace, G.; Wang, L.; Wishart, N. Design and Synthesis of Tricyclic Cores for Kinase Inhibition. *Bioorg. Med. Chem. Lett.* **2013**, *23*, 693−698.
(23) Gehringer, M.; Pfaffenrot, E.; Bauer, S.; Laufer, S. A. Design and Synthesis of Tricyclic JAK3 Inhibitors with Picomolar Affinities as Novel Molecular Probes. *ChemMedChem* **2014**, *9*, 277−281.
(24) Yamagishi, H.; Inoue, T.; Nakajima, Y.; Maeda, J.; Tominaga, H.; Usuda, H.; Hondo, T.; Moritomo, A.; Nakamori, F.; Ito, M.; Nakamura, K.; Morio, H.; Higashi, Y.; Inami, M.; Shirakami, S. Discovery of Tricyclic Dipyrrolopyridine Derivatives as Novel JAK Inhibitors. *Bioorg. Med. Chem.* **2017**, *25*, 5311−5326.
(25) Kim, M. K.; Shin, H.; Park, K.-s.; Kim, H.; Park, J.; Kim, K.; Nam, J.; Choo, H.; Chong, Y. Benzimidazole Derivatives as Potent JAK1-Selective Inhibitors. *J. Med. Chem.* **2015**, *58*, 7596−7602.
(26) Zak, M.; Mendonca, R.; Balazs, M.; Barrett, K.; Bergeron, P.; Blair, W. S.; Chang, C.; Deshmukh, G.; DeVoss, J.; Dragovich, P. S.; Eigenbrot, C.; Ghilardi, N.; Gibbons, P.; Gradl, S.; Hamman, C.; Hanan, E. J.; Harstad, E.; Hewitt, P. R.; Hurley, C. A.; Jin, T.; Johnson, A.; Johnson, T.; Kenny, J. R.; Koehler, M. F. T.; Bir Kohli, P.; Kulagowski, J. J.; Labadie, S.; Liao, J.; Liimatta, M.; Lin, Z.; Lupardus, P. J.; Maxey, R. J.; Murray, J. M.; Pulk, R.; Rodriguez, M.; Savage, S.; Shia, S.; Steffek, M.; Ubhayakar, S.; Ultsch, M.; van Abbema, A.; Ward, S. I.; Xiao, L.; Xiao, Y. Discovery and Optimization of C-2 Methyl Imidazopyrrolopyridines as Potent and Orally Bioavailable JAK1 Inhibitors with Selectivity over JAK2. *J. Med. Chem.* **2012**, *55*, 6176−6193.
(27) Soth, M.; Hermann, J. C.; Yee, C.; Alam, M.; Barnett, J. W.; Berry, P.; Browner, M. F.; Frank, K.; Frauchiger, S.; Harris, S.; He, Y.; Hekmat-Nejad, M.; Hendricks, T.; Henningsen, R.; Hilgenkamp, R.; Ho, H.; Hoffman, A.; Hsu, P.-Y.; Hu, D.-Q.; Itano, A.; Jaime-Figueroa, S.; Jahangir, A.; Jin, S.; Kuglstatter, A.; Kutach, A. K.; Liao, C.; Lynch, S.; Menke, J.; Niu, L.; Patel, V.; Railkar, A.; Roy, D.; Shao, A.; Shaw, D.; Steiner, S.; Sun, Y.; Tan, S.-L.; Wang, S.; Vu, M. D. 3-Amido Pyrrolopyrazine JAK Kinase Inhibitors: Development of a

DOI: 10.1021/acs.jmedchem.8b00510
J. Med. Chem. XXXX, XXX, XXX−XXX

JAK3 vs JAK1 Selective Inhibitor and Evaluation in Cellular and in Vivo Models. *J. Med. Chem.* **2013**, *56*, 345−356.
(28) Juchum, M.; Günther, M.; Döring, E.; Sievers-Engler, A.; Lämmerhofer, M.; Laufer, S. Trisubstituted Imidazoles with a Rigidized Hinge Binding Motif Act as Single Digit nM Inhibitors of Clinically Relevant EGFR L858R/T790M and L858R/T790M/C797S Mutants: An Example of Target Hopping. *J. Med. Chem.* **2017**, *60*, 4636−4656.
(29) Yao, W. C. F.; Burns, D. M.; Zhuo Azetidinyl Phenyl, Pyridyl or Pyrazinyl Carboxamide Derivatives as JAK Inhibitors. U.S. Patent US20170253598, 2017.
(30) Ferraccioli, R.; Carenzi, D.; Rombolà, O.; Catellani, M. Synthesis of 6-Phenanthridinones and Their Heterocyclic Analogues through Palladium-Catalyzed Sequential Aryl−Aryl and *N*-Aryl Coupling. *Org. Lett.* **2004**, *6*, 4759−4762.
(31) Yip, K.-T.; Yang, M.; Law, K.-L.; Zhu, N.-Y.; Yang, D. Pd(II)-Catalyzed Enantioselective Oxidative Tandem Cyclization Reactions. Synthesis of Indolines through C−N and C−C Bond Formation. *J. Am. Chem. Soc.* **2006**, *128*, 3130−3131.
(32) Trend, R. M.; Ramtohul, Y. K.; Stoltz, B. M. Oxidative Cyclizations in a Nonpolar Solvent Using Molecular Oxygen and Studies on the Stereochemistry of Oxypalladation. *J. Am. Chem. Soc.* **2005**, *127*, 17778−17788.
(33) Hagihara, M.; Izumi, N.; Tsuzaki, Y.; Matsugi, T.; Nakajima, T.; Hatano, M.; Hara, H. Novel Olefin Derivative. WO2005035501A1, 2005.
(34) Elsayed, M. S. A.; Griggs, B.; Cushman, M. Synthesis of Benzo[1,6]naphthyridinones Using the Catellani Reaction. *Org. Lett.* **2018**, *20*, 5228−5232.
(35) Villarino, A. V.; Kanno, Y.; Ferdinand, J. R.; O'Shea, J. J. Mechanisms of JAK/STAT Signaling in Immunity and Disease. *J. Immunol.* **2015**, *194*, 21−27.
(36) Kim, H.; Kim, M. K.; Choo, H.; Chong, Y. Novel JAK1-Selective Benzimidazole Inhibitors with Enhanced Membrane Permeability. *Bioorg. Med. Chem. Lett.* **2016**, *26*, 3213−3215.
(37) Korn, T.; Oukka, M.; Kuchroo, V.; Bettelli, E. Th17 Cells: Effector T Cells with Inflammatory Properties. *Semin. Immunol.* **2007**, *19*, 362−371.
(38) Manning, G.; Whyte, D. B.; Martinez, R.; Hunter, T.; Sudarsanam, S. The Protein Kinase Complement of the Human Genome. *Science* **2002**, *298*, 1912−1934.
(39) Smyth, L. A.; Collins, I. Measuring and Interpreting the Selectivity of Protein Kinase Inhibitors. *J. Chem. Biol.* **2009**, *2*, 131−151.
(40) Marlin, M. C.; Li, G. Biogenesis and Function of the NGF/TrkA Signaling Endosome. In *International Review of Cell and Molecular Biology*; Jeon, K. W., Ed.; Academic Press: Amsterdam, 2015; Vol. *314*, Chapter Six, pp 239−257.
(41) Park, J.; Kim, M.; Kang, S. G.; Jannasch, A. H.; Cooper, B.; Patterson, J.; Kim, C. H. Short-Chain Fatty Acids Induce Both Effector and Regulatory T Cells by Suppression of Histone Deacetylases and Regulation of the mTOR-S6K Pathway. *Mucosal Immunol.* **2015**, *8*, 80−93.

DOI: 10.1021/acs.jmedchem.8b00510
J. Med. Chem. XXXX, XXX, XXX−XXX